frontiers | Frontiers in Earth Science

TYPE Original Research
PUBLISHED 14 August 2024
DOI 10.3389/feart.2024.1441548

OPEN ACCESS

EDITED BY
Jianguo Zhang,
China University of Geosciences, China

REVIEWED BY
Chao Liang,
China University of Petroleum (East China), China
Qiqi Lyu,
Yangtze University, China

*CORRESPONDENCE
Laixing Cai,
qingxin717717@126.com

RECEIVED 31 May 2024
ACCEPTED 05 July 2024
PUBLISHED 14 August 2024

CITATION
Yuan C, Guo W, Cai L, Zeng Y, Zhang Z, Liu Y and Yang T (2024), Sedimentological and diagenetic facies of tight sandstones in lacustrine delta-front: A case study of the Jurassic Lianggaoshan Formation, eastern Sichuan Basin.
Front. Earth Sci. 12:1441548.
doi: 10.3389/feart.2024.1441548

Sedimentological and diagenetic facies of tight sandstones in lacustrine delta-front: A case study of the Jurassic Lianggaoshan Formation, eastern Sichuan Basin

Chengfang Yuan[1], Weixue Guo[1], Laixing Cai[1,2]*, Yangjing Zeng[3], Zhenkai Zhang[4], Yinglin Liu[1] and Tian Yang[1,2]

[1]Institute of Sedimentary Geology, Chengdu University of Technology, Chengdu, China, [2]State Key Laboratory of Oil and Gas Reservoir Geology and Exploitation, Chengdu University of Technology, Chengdu, China, [3]No. 5 Oil Production Plant, PetroChina Changqing Oilfield Company, Gaoling, China, [4]Shanxi Satellite Application Center for Natural Resources, Shanxi Institute of Geological Survey, Xi'an, China

In this study, taking the Jurassic Lianggaoshan Formation (J_1l) tight sandstones in the eastern Sichuan Basin as an example, the types and well-logging responses of main sedimentological and diagenetic facies in the lacustrine delta-front are investigated based on summarizing the sedimentary characteristics and reservoir properties. Subsequently, further validation and application are conducted in the study area through machine learning. Research results show that the J_1l lacustrine delta-front in the eastern Sichuan Basin mainly develops subaqueous distributary channels and mouth bar sand bodies, exhibiting typical densification reservoirs, with porosity and permeability distributed between 0.48% and 11.24% (av. 3.87%) and 0.0003–0.653 × 10^{-3} μm^2 (av. 0.026 × 10^{-3} μm^2), respectively. Strong compaction and strong cementation are the primary factors leading to densification, whereas chlorite coatings and weak dissolution play constructive roles in preserving some primary pores, creating a small amount of dissolution pores, and enhancing permeability. In terms of manifestation, the pore-throat content with a radius greater than 0.006 μm governs the reservoir quality. Furthermore, five types of diagenetic facies are identified in the J_1l subaqueous distributary channels and mouth bars: strong compaction facies (Type I), strong cementation facies (Type II), chlorite-coating and intergranular pore facies (Type III), weak dissolution and intragranular pore facies (Type IV), and medium compaction and cementation facies (Type V). Overall, the thick and coarse-grained subaqueous distributary channels can be considered as the preferred exploration targets for tight oil and gas, with type III and type IV diagenetic facies being the most favorable reservoirs, characterized by well-logging responses of high AC and low GR, DEN, and RT. Based on the fine division of sedimentological and diagenetic facies, establishing well-logging interpretation models and

then employing machine learning to achieve sweet spot reservoir prediction can provide valuable insights for tight oil and gas exploration in regions lacking core data.

KEYWORDS

sedimentological and diagenetic facies, well-logging response, machine learning method, tight sandstone, Lianggaoshan Formation, eastern Sichuan Basin

1 Introduction

Since the beginning of the 21st century, the petroleum industry worldwide has extended from conventional to unconventional fields, with the United States and China leading the development of unconventional hydrocarbon (Law and Curtis, 2002; Stephen, 2006; Külaots et al., 2010; Soeder, 2018; Zhu et al., 2019) and gradually forming the "symbiotic enrichment theory" of conventional–unconventional oil and gas (Zou et al., 2013; Yang et al., 2021; Jia et al., 2023). Currently, the recoverable resources of tight oil and gas account for approximately 40% and 45% of China's recoverable oil and natural gas resources, respectively (Sun et al., 2019; Zou et al., 2022). Compared to the nascent shale oil and gas and slowly developing coalbed methane, tight sandstones have emerged as a focus area for energy replacement in China, especially in the basins such as Ordos, Sichuan, Songliao, and Bohai Bay that have achieved remarkable exploration achievements (Jia et al., 2018; Dai et al., 2021; Guo et al., 2022; Wang et al., 2023). As a crucial carrier for hydrocarbon migration and accumulation, tight sandstones consistently stand at the forefront and core of reservoir geological research; that is, the central objective of seeking oil–gas accumulation zones is to locate the reservoir sweet spots.

In the absence of tectonic activity, reservoir quality is jointly influenced by the original sedimentary environment and later diagenetic reconstruction, exhibiting a pattern of "facies control" (Haile et al., 2018; Yang et al., 2021; Alam et al., 2022; Kra et al., 2022). Sedimentary processes control the spatial distribution of sand bodies, and the original reservoir properties are determined through rock composition and texture characteristics, such as initial mineral composition, particle size, and sorting (Khalifa and Morad, 2015; Bahrehvar et al., 2021; Lai et al., 2023). After entering the burial environment, the sediments not only undergo continuous mechanical compaction but also pass through a series of water–rock reactions to modify the material and pore distribution, ultimately forming the current reservoir characteristics, known as diagenetic facies. Moreover, there is a spatiotemporal correlation between diagenetic facies and sedimentary facies, which means that there is certain regularity in the distribution of diagenetic facies within sand bodies (Henares et al., 2014; Zhang et al., 2014; Wang et al., 2017).

Early diagenetic facies were proposed as an important approach to solve the diagenesis and heterogeneity in carbonate reservoirs (Packham and Keith, 1960; Railsback, 1984). Later, it was continuously supplemented and developed in research on sandstone reservoirs, but a unified concept and division scheme have not yet been formed. Railsback (1984) regarded diagenetic facies as rock masses or geological units with different diagenetic textures, and after being introduced into China, this concept was extended to a comprehensive representation of diagenetic environments and products, encompassing the sum of petrological, geochemical, and petrophysical characteristics (Chen and Liu, 1994). To date, many scholars emphasize that diagenetic facies are physical manifestations reflecting the diagenetic environment (Carvalho et al., 1995; Dill et al., 2005; Zheng et al., 2007; Zou et al., 2008; 2013; Lai et al., 2018). This includes the aforementioned diagenetic products as well as the intensity of diagenetic events revealed by them, including comprehensive characteristics such as rock particles, cement types, petrofabrics, pores, and fractures (Zou et al., 2008; He et al., 2011). Moreover, due to differences in classification criteria, there is no convention for naming diagenetic facies. Factors such as reservoir lithology, porosity and permeability, pore type, diagenetic event, and the intensity and combination of diagenesis are all involved in this context (Cao et al., 2015; Mou et al., 2016; Lai et al., 2019; Fang, 2020; Wu et al., 2020; Li et al., 2022). However, the common understanding is that the diagenetic facies, based on revealing the current characteristics and genesis of reservoirs, summarize the regional diagenetic evolution patterns (Cui et al., 2017; Liu et al., 2018; Lai et al., 2019; Li et al., 2020). Well-logging data record multiple information such as mineral composition, lithological combination, pore structure, porosity, and permeability in rocks, with outstanding characteristics of good vertical continuity, high resolution, and low economic cost, providing a scientific basis for identifying diagenetic facies in sections lacking core samples (Lai et al., 2020; Wu et al., 2020; Li et al., 2022; Zhao et al., 2022). The widely used methods based on well-logging data include cross-plot, spider chart, mathematical analyses (Fisher discriminant analysis and factor analysis), and neural network algorithms (probabilistic neural network and BP neural network) (Lai et al., 2018; 2019; Li et al., 2022; Zhao et al., 2022; Zheng et al., 2022).

The tight sandstones of Lower Jurassic Lianggaoshan Formation (J_1l) have become a new exploration focus in the Sichuan Basin, owing to its shallow burial and low exploration costs (Zhang, 2021; Zhang and Yang, 2022; Cheng et al., 2023a). Previous studies have indicated that the geological resources of the J_1l tight gas in the eastern Sichuan Basin reach 2.0×10^8t, and abundant hydrocarbon shows, including industrial oil and gas flows, have been discovered in over 50 wells (Zou et al., 2018; Zhang, 2021; Yi et al., 2022). In view of the heterogeneity of the reservoir of the J_1l tight sandstones, containing differences in porosity and permeability, pore–throat structure, and diagenesis, this study investigates the joint control of sedimentological and diagenetic facies on reservoir quality. This not only contributes to understanding the mechanisms and processes of reservoir densification but also accurately serves as the optimization of exploration targets.

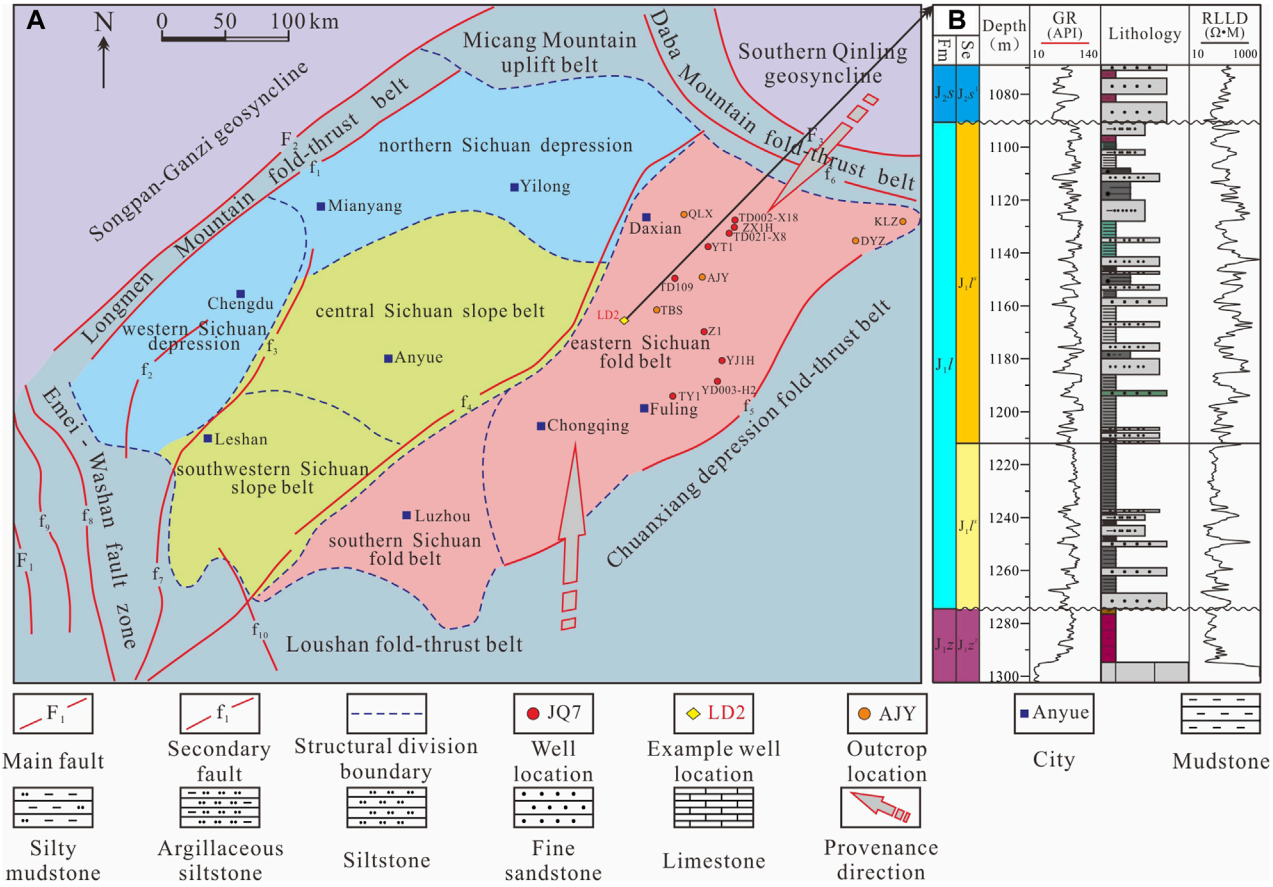

FIGURE 1
Structural divisions of the Sichuan Basin **(A)** and the J_1l stratigraphic characteristics in well LD2, eastern Sichuan Basin **(B)**. F_1, Anninghe fault; F_2, Longmen Mountain fault; F_3, Chengkou fault; f_1, Pengguan fault; f_2, Xiongpo fault; f_3, Longquan Mountain fault; f_4, Huaying Mountain fault; f_5, Qiyue Mountain fault; f_6, Wanyuan fault; f_7, Emei–Washan fault; f_8, Hanyuan fault; f_9, Puxiong river fault; f_{10}, Yadu-Mashan fault.

2 Regional geological background

The Sichuan Basin is located in the northwest of the Yangtze Plate and is a large superimposed basin based on rigid granite, with abundant marine and continental petroleum resources (Korsch et al., 1991; Yokoyama et al., 2001; Wang CY. et al., 2022; He, 2022). The periphery of the basin is surrounded by the Longmen Mountain fold–thrust belt, Micang Mountain uplift belt, Daba Mountain fold–thrust belt, Chuanxiang depression fold–thrust belt, Loushan fold–thrust belt, Emei–Washan fault zone (Zhao et al., 2012; Wang et al., 2020; Huang et al., 2023; Kane et al., 2023). In addition, the interior of the basin is divided into six secondary structural units: western Sichuan depression, northern Sichuan depression, central Sichuan slope belt, southwestern Sichuan slope belt, southern Sichuan fold belt, and eastern Sichuan fold belt (Zhu et al., 2018; Wang XJ. et al., 2022; Figure 1A). Among them, the eastern Sichuan fold belt is separated from the central Sichuan slope belt by the Huaying Mountain fault, bordering the Daba Mountain fold–thrust belt in the north and the South China fold system in the southeast (Figure 1A).

Under the tectonic setting of compressional orogeny following the Indosinian Movement (Şengör, 1985; Xu et al., 2012), the Micang Mountain and Daba Mountain in the northeast margin of the basin rapidly uplifted in the early Jurassic and transported a large amount of terrigenous clastics into the basin as the main provenance areas (Li et al., 2018; Meng et al., 2022; Cheng et al., 2023b). Additionally, the secondary provenance area known as the Xuefeng uplift is developed in the southeastern part of the basin (Zheng et al., 2019; Cheng et al., 2023b). Against the backdrop of multiple transitions from shallow to semi-deep lake depositional environments, the Jurassic system in the eastern Sichuan Basin is successively developed from the bottom to top as follows: the Ziliujing Formation (J_1z), Lianggaoshan Formation (J_1l), and Shaximiao Formation (J_2s), with widespread delta sedimentary facies in J_1l (Wang ZC. et al., 2022; Yi et al., 2022; Cheng et al., 2023a; Yu et al., 2023). Under the comprehensive control of factors such as paleoclimate change, lake-level fluctuation, and ancient source supply, the mudstones of the prodelta and semi-deep lake are vertically superimposed with the sandstones of delta front, forming a favorable configuration of hydrocarbon source rocks and reservoirs (Figure 1B).

3 Samples and testing methods

3.1 Sample collection

Based on the core observation of six wells (TD021-X8, TD109, YT1, YD003-H2, ZX1H, and YJ1H) in the eastern Sichuan Basin, this study additionally supplemented five outcrops to summarize the sedimentary characteristics, namely, QLX (107°44′37″E, 31°11′49″N), TBS (107°31′32″E, 30°36′1″N), AJY (107°52′20″E, 30°47′52.2″N), DYZ (109°1′31.2″E, 30°59′44.4″N), and KLZ (109°28′49.2″E, 31°5′41.5″N) profiles (Figure 1A). All the samples were taken from intact block rocks on the core and outcrop, and all the samples were sandstone, except mudstone for major and trace elements. A total of 605 samples were tested at the State Key Laboratory of Oil and Gas Reservoir Geology and Exploitation (Chengdu University of Technology), including 63 casting thin sections, 173 particle-size analyses, 174 X-ray diffraction (XRD) analyses, 14 whole-rock major and trace elements, 10 scanning electron microscopic (SEM) observations, 16 high-pressure mercury injection (HPMI) analyses, and 155 porosity and permeability testing.

3.2 Testing methods

3.2.1 Analyses of minerals and rocks

According to the rock thin-section preparation standard SY/T 5913-2021 of China's petroleum and gas industry, rock samples were polished to a thickness of approximately 0.03 mm and stained with a mixed solution of alizarin Red S and potassium ferrocyanide to prepare casting thin sections. The mineral composition and structure of rocks were then observed using a Zeiss AxToScope.A1ApoL polarizing microscope. XRD testing requires first grinding the dried sample to a particle size smaller than 200 mesh and later obtaining the spectrum using a D/Max-2500 X-ray diffractometer, with specific testing conditions of 1° emission slit, 0.3 mm receiving slit, 2°/min scanning speed, and 0.02° sampling width. In response to the fine-grained rocks in the study area, particle size analyses were conducted in accordance with the standard of SY/T 5434-2018, using an APA2000 laser particle size analyzer as the testing instrument. In addition, the major element determination was carried out using an Axios PW4400 X-ray fluorescence spectrometer, and the trace elements were conducted using a Thermo XSERIES 2 inductively coupled plasma mass spectrometry (ICP-MS), both with an analysis accuracy of ±5%.

3.2.2 Analyses of reservoir characteristics

The porosity and permeability related to reservoir evaluation were tested following the core analysis practices of the standard SY/T 5913-2006, using instruments such as the UltraPore-200 A helium porosimeter and ULTRA-PERM^{TM}200 permeameter, respectively. SEM testing was performed under an FEG 450 scanning electron microscope to identify mineral types and pore morphology, with the standard of GB/T 18295-2001. The minimum pore radius measured using the AutoPore IV 9505 mercury porosimeter can reach 5 nm, which is suitable for characterizing the pore–throat structure of tight sandstones (Cai et al., 2019; Zhang et al., 2019).

4 Results

4.1 Sedimentary characteristics

4.1.1 Marks of sedimentary facies identification

Rock colors: in the eastern Sichuan Basin, the J_1l cores and outcrops display a rich variety of rock colors, including reduced colors such as black, grayish black, and dark gray, as well as reddish brown, grayish green, and grayish white formed in oxidizing conditions (Figures 2A–C). Meanwhile, the color of mudstones changes regularly, from grayish black and dark gray in the J_1l^x segment to gray, grayish green, and reddish brown in the J_1l^s segment (Figure 1B), indicating that the J_1l water body is shifting from deep to shallow and frequent small-scale lake transgression and regression cycles.

Petrology characteristics: the content of the argillaceous matrix in the J_1l sandstones ranges from 2% to 9%, with an average value of about 6%, making it an arenite. Thin sections show that the particle sizes are relatively fine, distributed in the range of 0.06–0.25 mm, and the rocks exhibit a particle-supported texture, with moderate sorting and a sub-rounded to hypo-edge angle in roundness (Figure 2D). The main types of sandstones are feldspathic litharenite and lithic arkose (Figure 2E). Among them, the content distribution ranges of quartz, feldspar, and rock debris are 52.53%–66.22%, 13.40%–26.46%, and 17.35%–29.29%, with the average contents of 56.50%, 22.42%, and 21.08%, respectively. Furthermore, in terms of rock debris types, sedimentary rock is predominant, with a relative content of 47.67%, followed by metamorphic rock, with a relative content of 44.96% (Figure 2F).

XRD testing of the core and AJY outcrop samples further revealed the mineral characteristics of "high content of quartz and feldspar, as well as low content of calcite and dolomite." In sandstones, the quartz content generally ranges from 26.3% to 88.4% (av. 52.98%), and the contents of plagioclase and K-feldspar account for 0.7%–38.4% (av. 21.79%) and 1.4%–23.2% (av. 6.38%), respectively. Correspondingly, the average contents of calcite and dolomite are only 2.2% and 0.59%, respectively (Table 1). The content of clay minerals is distributed between 8.3% and 36.1%, with an average value of 18.03%. Combined with the lower content of the argillaceous matrix, it reflects a stronger cementation of clay minerals in the later diagenetic stage. Kaolinite is commonly developed in clay minerals, with a content range of 6.4%–47.0% and an average content range of 20.41%. Chlorite and illite are quite similar, with average contents of 16.4% and 15.0%, respectively. In addition, minerals such as siderite, pyrite, and anhydrite are rare, and their contents generally do not exceed 1.4% (Table 1).

Sedimentary structures: in the J_1l sandstones, bedding structures characterized by abundant trough cross-bedding (Figure 3A) and parallel bedding (Figure 3B) reflect strong hydrodynamic conditions. Additionally, wedge-shaped cross-bedding (Figure 3C), wavy bedding (Figure 3D), and flaser bedding (Figure 3E) can also be observed, revealing the hydrodynamic forces of waves and tides. Oblique bedding in fine sandstones is interbedded with the horizontal bedding in mudstones (Figure 3F), indicating the alternating variations in sediment dynamics. As the river energy gradually weakens, fine-grained sediments such as siltstones and argillaceous siltstones form wave-ripple bedding and climbing ripple bedding under the repeated wave erosion

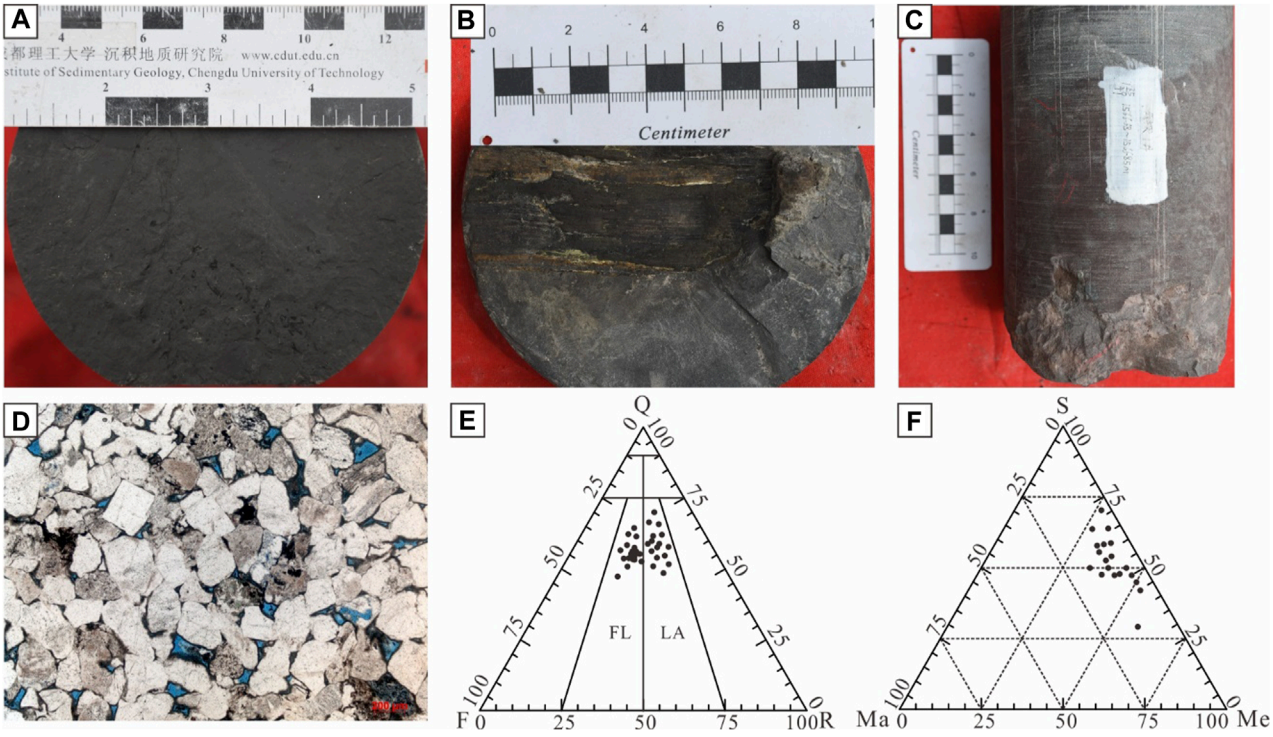

FIGURE 2
Petrology characteristics of the J_1l tight sandstones in the eastern Sichuan Basin. **(A)** Well ZX1H, 1891.4 m, J_1l^x segment, grayish black mudstone; **(B)** well TD109, 1328.9 m, J_1l^s segment, gray mudstone; **(C)** well YT1, 1566.8 m, J_1l^s segment, grayish green and reddish brown silty mudstone; **(D)** well ZX1H, 1817.36 m, J_1l^s segment, fine sandstone with a moderate sorting and hypo-edge angle in roundness; **(E)** triangular diagram for the classification of sandstones (Q, quartz; F, feldspar; R, rock debris; FL, feldspathic litharenite; and LA, lithic arkose); and **(F)** triangular diagram for the classification of rock debris (S, sedimentary rock; Ma, magmatic rock; and Me, metamorphic rock).

(Figure 3G), often accompanied by reverse grading. Due to the erosion of the overlying sandstone into the underlying mudstone, a bottom surface of scour is formed (Figure 3H), which usually indicates the presence of strong hydrodynamic channel deposition. Additionally, flame structure, ball–pillow structure, and convolute bedding are also common deformation structures near the sand–mud contact surface (Figures 3I, J). Fossils and bioglyphs are developed in the study area, such as Muschel sandstone (Figure 3K), shell mudstone (Figure 3L), bioturbation structure (Figure 3M), and phytoclast (Figure 3N), which further confirm the sedimentary background of shallower water and nearby provenance.

4.1.2 Sedimentary environments

Geochemical methods are widely used in the restoration and reconstruction of sedimentary environments. For example, the values of Sr/Cu, Rb/Sr, K_2O/Al_2O_3, and paleoclimate index C are considered as effective indicators for discussing paleoclimate (Beckmann et al., 2005; Moradia et al., 2016; Cai et al., 2023). The ratio of metal elements such as V, Cr, Co, and Ni can be used to distinguish paleo-redox conditions, and parameters like Sr/Ba and Rb/K are employed to characterize the paleosalinity of water bodies (Jones and Manning, 1994; Wei and Thomas, 2020). In addition, the relative contents of elements Al and Ti are applied to analyze the input intensity of terrigenous clastics (Greber and Dauphas, 2019; Han et al., 2022).

In the J_1l^x segment, K_2O/Al_2O_3 values are all below 0.2, with a maximum value of 0.188, indicating an overall warm and humid paleoclimate. The paleoclimate index C values are relatively large, especially for the lower three samples, all of which exceed 0.80 with an average value of 1.02, further confirming this conclusion. The test results of the J_1l^s 11 rock samples show that the distribution range of K_2O/Al_2O_3 values slightly increases to 0.165–0.270, with an average value of 0.205, and the paleoclimate index C values decrease to 0.59–0.86, with an average value of 0.76, both revealing the development of a semi-humid to semi-arid climate. Overall, the paleoclimate transitioned from warm and humid to later semi-humid conditions. After experiencing a short-term dry heat fluctuation, the characteristics of drought and heat are obvious in the early stage of J_2S (Figure 4).

According to the V/Cr parameter boundary proposed by Jones and Manning (1994), the J_1l sedimentary water body can be divided into two stages: hypoxic environment and oxygen-rich environment (Figure 4). In the J_1l^x segment, except for the bottom sample with a V/Cr value of 1.25, the V/Cr values of the other samples range from 1.56 to 4.63, with an average of 2.37, indicating a typical reducing environment. In the later stage, the V/Cr values of the J_1l^s samples significantly decrease to the range of 1.50–2.29, with an average value of 1.73, reflecting the transition of the water body from hypoxia to relatively oxygen enrichment. The variation trend of Ni/Co values is similar to that of V/Cr values, which also reveals the difference in the oxygen content of the water, but all the Ni/Co values

TABLE 1 XRD test results of the J_1l tight sandstones in the eastern Sichuan Basin.

Sample no.	Depth (m)	Relative content of ordinary non-clay mineral (%)								Relative content of clay mineral (%)					
		Quartz	K-feldspar	Plagioclas	Calcite	Dolomite	Siderite	Pyrite	Anhydrite	Total content	Kaolinite	Chlorite	Illite	I/S	C/S
AJY04	54.5	88.4	—	0.7	2.6	—	—	—	—	8.3	21.9	23.7	19.4	20.5	14.5
AJY12	113.5	51.7	2.9	21.3	1.9	0.1	0.4	—	—	21.7	47.0	6.6	19.7	15.0	11.7
AJY18	196.4	60.9	1.4	16.9	0.2	0.2	—	—	—	20.4	24.4	7.9	16.6	14.6	36.5
AJY23	223.0	59.3	5.0	25.1	0.2	1.4	—	—	—	9.0	6.4	11.9	8.6	1.8	71.3
AJY26	232.0	32.4	23.2	31.2	0.3	—	—	—	1.2	11.7	11.4	14.5	15.7	11.8	46.6
AJY28	242.5	35.9	10.1	36.7	0.2	—	0.4	—	1.4	15.3	12.0	18.3	11.3	12.8	45.6
AJY49	405.5	44.5	1.8	36.7	0.2	—	—	0.3	—	16.5	19.8	32.1	13.9	21.3	12.9
YJ1H01	2010.0	40.5	—	16.5	6.9		—	—	—	36.1	—	—	—	—	—
YJ1H02	2034.0	42.0	—	17.2	11.7	0.5	—	—	—	28.6	—	—	—	—	—
ZX1H01	1764.8	58.2	9.9	21.9	1.1	0.4	—	—	—	8.5	—	—	—	—	—
ZX1H02	1766.2	26.3	3.9	38.4	—	—	—	—	—	31.4	—	—	—	—	—
ZX1H03	1767.7	61.7	3.0	22.2	0.3	—	—	—	—	12.8	—	—	—	—	—
ZX1H04	1769.2	48.1	3.4	31.1	0.8	0.6	—	—	—	16.0	—	—	—	—	—
ZX1H05	1770.9	63.6	4.5	14.7	—	—	—	—	—	17.2	—	—	—	—	—
ZX1H06	1775.6	51.3	2.2	15.0	1.4	—	—	—	—	30.1	—	—	—	—	—
ZX1H07	1777.1	59.2	1.7	11.8	—	—	—	—	—	27.3	—	—	—	—	—
ZX1H08	1817.2	60.9	8.3	17.4	0.5	—	—	—	—	12.9	—	—	—	—	—
ZX1H09	1818.3	54.9	4.2	25.9	1.6	0.7	—	—	—	12.7	—	—	—	—	—
ZX1H10	1820.9	61.7	2.7	17.3	0.9	0.5	—	—	—	16.9	—	—	—	—	—
ZX1H11	1823.3	50.2	3.3	28.3	3.1	—	—	—	—	15.1	—	—	—	—	—
ZX1H12	1824.3	57.8	4.0	21.7	0.9	0.7	1.3	—	—	13.6	—	—	—	—	—

(Continued on the following page)

10.3389/feart.2024.1441548

10.3389/feart.2024.1441548

TABLE 1 (*Continued*) XRD test results of the J_1l tight sandstones in the eastern Sichuan Basin.

Sample no.	Depth (m)	Relative content of ordinary non-clay mineral (%)									Relative content of clay mineral (%)					
		Quartz	K-feldspar	Plagioclase	Calcite	Dolomite	Siderite	Pyrite	Anhydrite	Total content	Kaolinite	Chlorite	Illite	I/S	C/S
ZX1H13	1825.5	45.0	13.4	23.2	0.6	—	—	—	—	17.8	—	—	—	—	—
ZX1H14	1826.9	35.3	18.6	23.1	—	0.8	—	—	—	22.2	—	—	—	—	—
ZX1H15	1895.5	59.5	—	15.9	7.6	—	—	—	—	17.0	—	—	—	—	—
ZX1H16	1897.5	66.6	—	16.2	3.2	—	—	—	—	14.0	—	—	—	—	—
ZX1H17	1907.5	61.8	—	20.3	2.3	—	—	—	—	15.6	—	—	—	—	—

are smaller than the previous boundary of 5.00 between poor and rich oxygen. On the one hand, this implies that the oxygen content in the study area is relatively low but still insufficient to be clearly defined as hypoxic conditions. On the other hand, this may reflect certain differences in the sedimentary response of continental and marine basins.

The paleosalinity can also be divided into two evolutionary stages: the J_1l^x segment characterized by salt water and the J_1l^s segment characterized by brackish water (Figure 4). The Sr/Ba value of the sample in the 6th sub-layer is relatively low, at 0.327, and then rapidly increases to 2.24 in the 21st sub-layer. Contrary to it, the Rb/K value gradually decreases from 0.007 at the bottom to 0.001, providing further confirmation of the brackish water environment. Form the J_1l^s period to the early J_2s stage, the distribution range of Sr/Ba values is 0.078–0.372, with an average value of 0.157, and the Rb/K values range from 0.004 to 0.007, with an average value of 0.005. Two types of parameters indicate that the water salinity decreased, with brackish water being the main component.

Under the warm and humid paleoclimate background of the early J_1l Formation, the Si/Al and Ti/Al values in the J_1l^x segment decreased significantly, which indicates relatively weak input intensity of terrigenous clastics, dropping from 3.176 to 0.063 in the 9th layer to 3.092 and 0.046 in the 21st layer, respectively. Controlled by the overall lake regression in the J_1l^s segment, the sand bodies show significant progradation characteristics. The Si/Al and Ti/Al values of the J_1l^s samples are distributed in the ranges of 2.703–3.365 and 0.037–0.052, with average values of 3.118 and 0.048, respectively, which are slightly higher than those in the J_1l^x segment (Figure 4).

4.2 Reservoir qualities

4.2.1 Porosity and permeability

A total of 155 measured data of the J_1l sandstones reveal that the porosity (Φ) and permeability (K) range from 0.48% to 11.24% and from 0.0003×10^{-3} μm^2 to 0.653×10^{-3} μm^2, with average values of 3.87% and 0.026×10^{-3} μm^2. Among them, the samples with porosity less than 6% account for 71.0% and the samples with permeability less than 0.05×10^{-3} μm^2 account for 91% (Figure 5A), indicating typical tight and ultra-tight sandstone reservoirs. In addition, there is a significant positive correlation between porosity and permeability as a whole, and there are two types of abnormal cases. Type A is characterized by low porosity with relatively high permeability, which may be due to the presence of micro-fractures enhancing the reservoir's permeability. Type B is characterized by relatively high porosity with low permeability, suggesting that the reservoir space may be dominated by primary pores (Figure 5A). Excluding the two types of abnormal data, the positive correlation coefficient of the remaining porosity and permeability data is about 0.0428.

4.2.2 Pore-throat structures

Consistent with low porosity, reservoir spaces of the J_1l sandstones are generally underdeveloped, primarily comprising original intergranular pores, secondary dissolution pores, and a few micro-fractures (Zhang et al., 2022; Yu et al., 2023). The micron

FIGURE 3
Sedimentary structures of the J_1l tight sandstones in the eastern Sichuan Basin. **(A)** Well YD003-H2, 2104.3 m, J_1l^S segment, trough cross-bedding; **(B)** KLZ outcrop, J_1l^S segment, parallel bedding; **(C)** KLZ outcrop, J_1l^S segment, wedge-shaped cross bedding; **(D)** KLZ outcrop, J_1l^S segment, wavy bedding; **(E)** well YT1, 2167.3 m, J_1l^S segment, flaser bedding; **(F)** TBS outcrop, J_1l^X segment, oblique bedding and horizontal bedding; **(G)** well ZX1H, 1909.3 m, wave-ripple bedding; **(H)** well TD021-X8, 1800.62 m, J_1l^S segment, bottom surface of scour; **(I)** well TD109, 1330.9 m, ball–pillow structure; **(J)** well TD109, 1331.1 m, convolute bedding; **(K)** KLZ outcrop, J_1l^X segment, Muschel sandstone; **(L)** well ZX1H, 1896.9 m, J_1l^X segment, shell mudstone; **(M)** well YT1, 2152.3 m, J_1l^S segment; and **(N)** well YT1, 2152.3 m, J_1l^S segment, phytoclast.

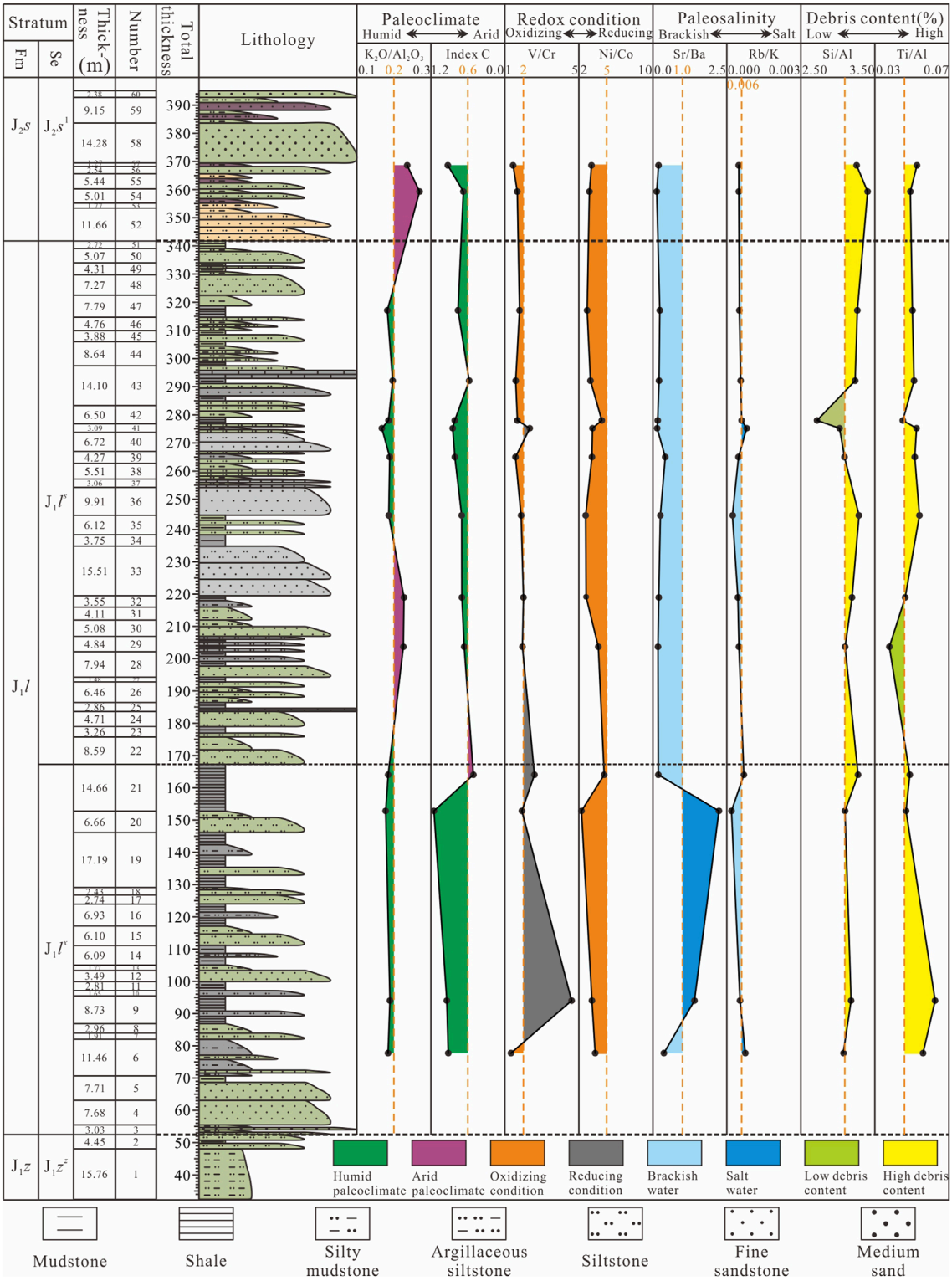

FIGURE 4
Geochemical profile and depositional environment of J_1l in AJY outcrop, eastern Sichuan Basin.

pores are connected by nanoscale throats, and the maximum pore-throat radius is 1.085 μm. The mean values of pore-throat radii are distributed in the range of 0.011–0.09 μm, and the median values range from 0.007 to 0.163 μm (Figure 5B). Meanwhile, the sorting coefficient and homogeneity coefficient of pore-throat structures are concentrated within the ranges of 0.99–2.27 and 0.22–0.31, with

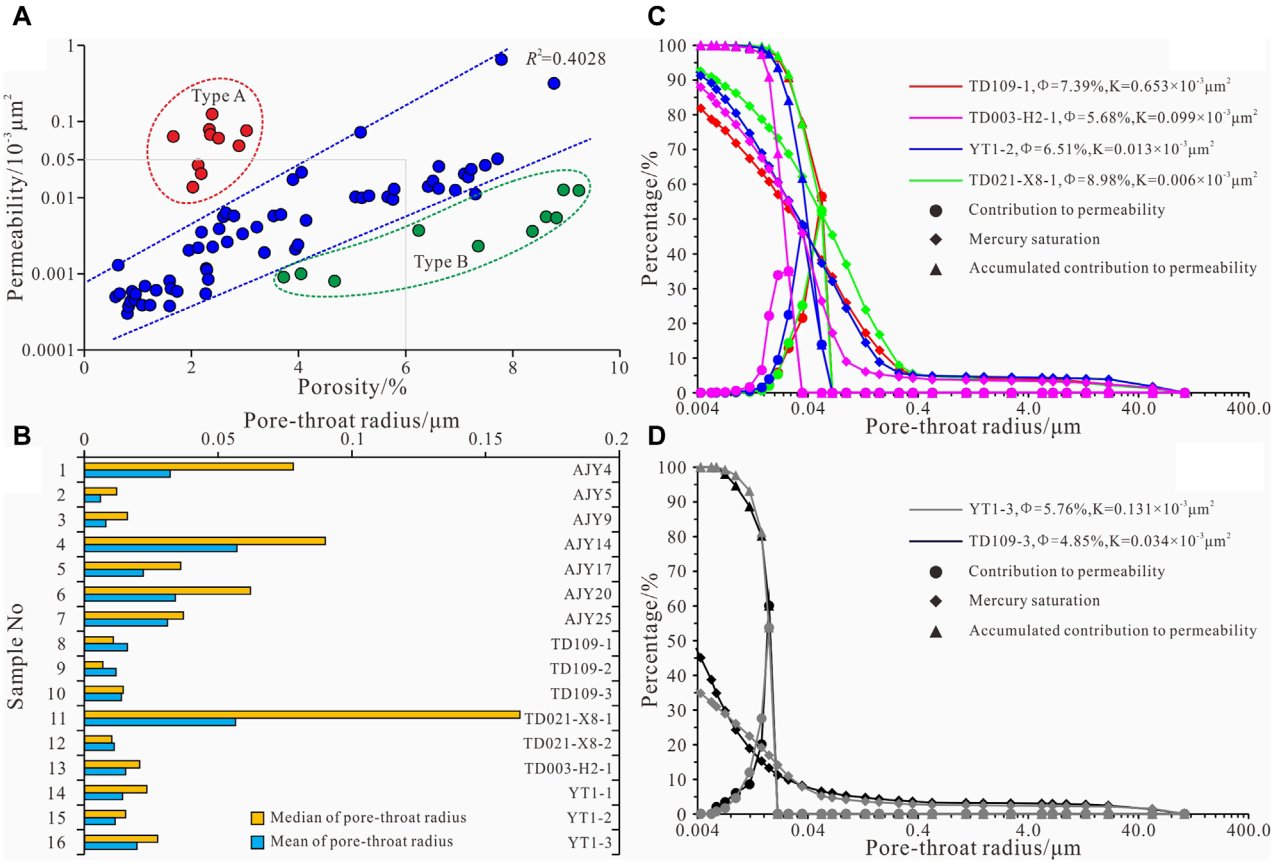

FIGURE 5
Reservoir properties and pore-throat structures of the J_1l tight sandstones in the eastern Sichuan Basin. **(A)** Distribution characteristics of porosity and permeability; **(B)** distribution characteristics of pore-throat radius; **(C)** pore-throat structures of relatively favorable reservoirs; and **(D)** pore-throat structures of relatively poor reservoir.

average values of 1.67 and 0.25, respectively, indicating that the pores and throats are not only tiny but also poorly sorted and highly heterogeneous. Comparing the samples with significant differences in mercury saturation, it is found that the oil saturation of tight sandstones is positively correlated with porosity and permeability but fundamentally depends on the maximum throat radius. For example, in Figures 5C, D, the samples with a mercury saturation of 83.7%–93.9% exhibit pore-throat radii ranging from 0.006 to 0.053 μm, whereas radii of the samples with a mercury saturation of 36.5%–49.4% are significantly reduced to 0.006–0.018 μm. However, the common feature is that the permeability of all samples is mainly contributed by the larger pore-throats. In contrast, the pore-throats with smaller radii may accumulate relatively large volumes but limited contribution to permeability.

5 Discussions

5.1 Sedimentological and diagenetic facies

5.1.1 Types and characteristics of sedimentary micro-facies in lacustrine delta-front

Under the continuous debris supply from the two provenance systems in the northeastern and southeastern Sichuan Basin (Yi et al., 2022; Cheng et al., 2023a; 2023b; Figure 1), sand bodies of the delta-front sub-facies are widely distributed in the study area, and the sedimentary micro-facies such as subaqueous distributary channels (SDC), mouth bars (MB), and sheet sands (SS) can be identified (Figure 6).

As the framework of the delta-front, the subaqueous distributary channels mainly deposit fine sandstones and siltstones, with obvious normal-graded bedding and bottom surface of scour (Figures 3H, 6). Vertically, the superposition of multiple channels creates a thick composite sand body, whose thickness and scale are controlled by the intensity and duration of flowing water, presenting a box-shaped or bell-shaped well-logging curve (Figure 6). On the plane, the channels extend far, and trough cross-bedding, wedge-shaped cross-bedding, and parallel bedding are often developed in the sand bodies, with common deformation structures (Figure 3).

After the fine-grained debris carried by the river enters the lake, it accumulates at the estuaries and forms mouth bars as the flow velocity decreases. The thickness of a single sand body is approximately 0.3–2.0 m, with reverse grading and swash bedding as typical identification marks (Figures 3G, 6). At the same time, bioturbation structures and shell layers can also be observed (Figure 3K), and the well-logging curve is generally funnel shaped (Figure 6). The sheet sand has the

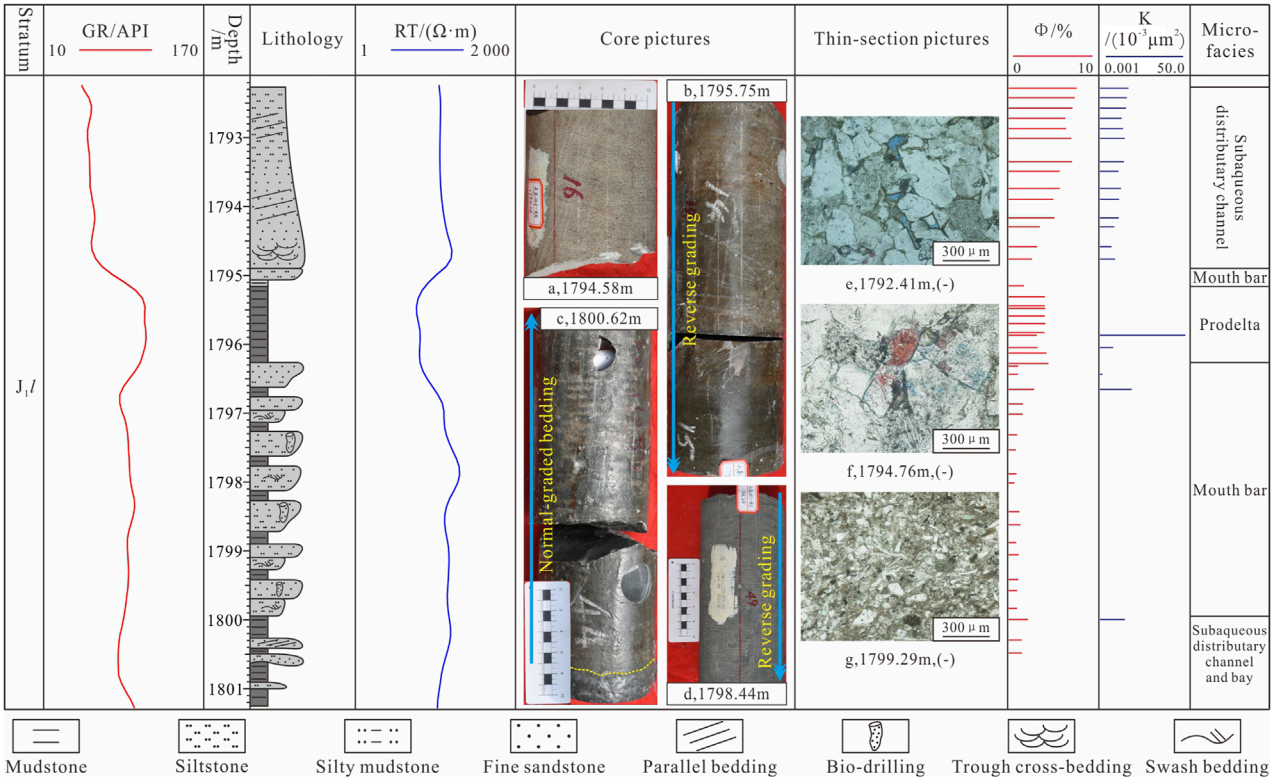

FIGURE 6
Sedimentary facies profile of the J_1l tight sandstones in well TD021-X8 in the eastern Sichuan Basin. Pic. a. 1794.58 m, trough cross-bedding; Pic. b. 1795.75 m, reverse grading; Pic. c. 1800.62 m, bottom surface of scour and normal-graded bedding; Pic. d. 1798.44 m, reverse grading; Pic. e. 1792.41 m, original intergranular pores; Pic. f. 1794.76 m, secondary dissolution pores; and Pic. g. 1799.29 m, argillaceous siltstone under strong compaction.

same structure as the mouth bars, with extensive cross-bedding but few biological fossils.

5.1.2 Types and characteristics of diagenetic facies in lacustrine delta-front

There are various types and multiple stages of diagenesis in the study area, and compaction and carbonate cementation are the most prominent and destructive to the reservoir quality. Although chlorite coatings and dissolution processes have increased the porosity and permeability to some extent, their effects are not significant. The relatively finer particles and higher content of the argillaceous matrix lead to strong compaction of the rock, with the particles exhibiting an overall linear contact relationship (Figure 7A), and the mica and debris particles are deformed due to compression (Figure 7B). After staining, calcite cement appears red under the microscope, filling intergranular pores and secondary dissolution pores (Figures 7C, D). It is found that the lowest and highest temperatures of fluid inclusions in calcite cement are 57.9° and 125°, respectively (Liu AQ. et al., 2023; Figure 7E), with the majority occurring in the late stages and often within the sand bodies near mudstones. The siliceous cementation event also occurs in two stages, and the thickest enlarged edge with a thickness of 1 mm mainly fills intergranular pores (Figure 7F). The chlorite coatings are usually formed before siliceous cementation and can even be considered one of the earliest diagenetic events, coexisting with intergranular pores (Figure 7G). This may be because the chlorite coatings resist a certain degree of compaction and pressolution (Ehrenberg, 1993; Bloch et al., 2002; Huang et al., 2021) and also hinder the contact between particles and pore fluids (Cho and Fawcett, 1986; Ehrenberg, 1993; Worden et al., 2020). However, the abundant intercrystalline pores in clay minerals may not completely prevent the exchange of matter and energy between pore fluids and particle surfaces. For instance, the feldspar wrapped in chlorite coatings can also undergo dissolution (Figure 7H), as can the siliceous nodules growing on chlorite flakes (Figure 7I).

Based on the reference of particle contact relationship and strength (Formula 1; Mou et al., 2017), pore-throat structure, and plane porosity, the three parameters, namely, the apparent compaction rate, apparent cementation rate, and apparent dissolution rate, are calculated according to Formulas 2–5 (Beard and Weyl, 1973; Yang et al., 2014; Lai et al., 2018; 2023; Liu HK. et al., 2023). Furthermore, the compaction, cementation, and dissolution are classified into three levels: strong, medium, and weak (Table 2).

$$\text{Contact Intensity(CI)} = \frac{1a + 1.5ab + 2b + 3c + 4d}{a + ab + b + c + d}, \quad (1)$$

where “a” represents the number of samples with point contact particles, “b” represents the number of samples with point-line contact particles, “c” represents the number of samples with

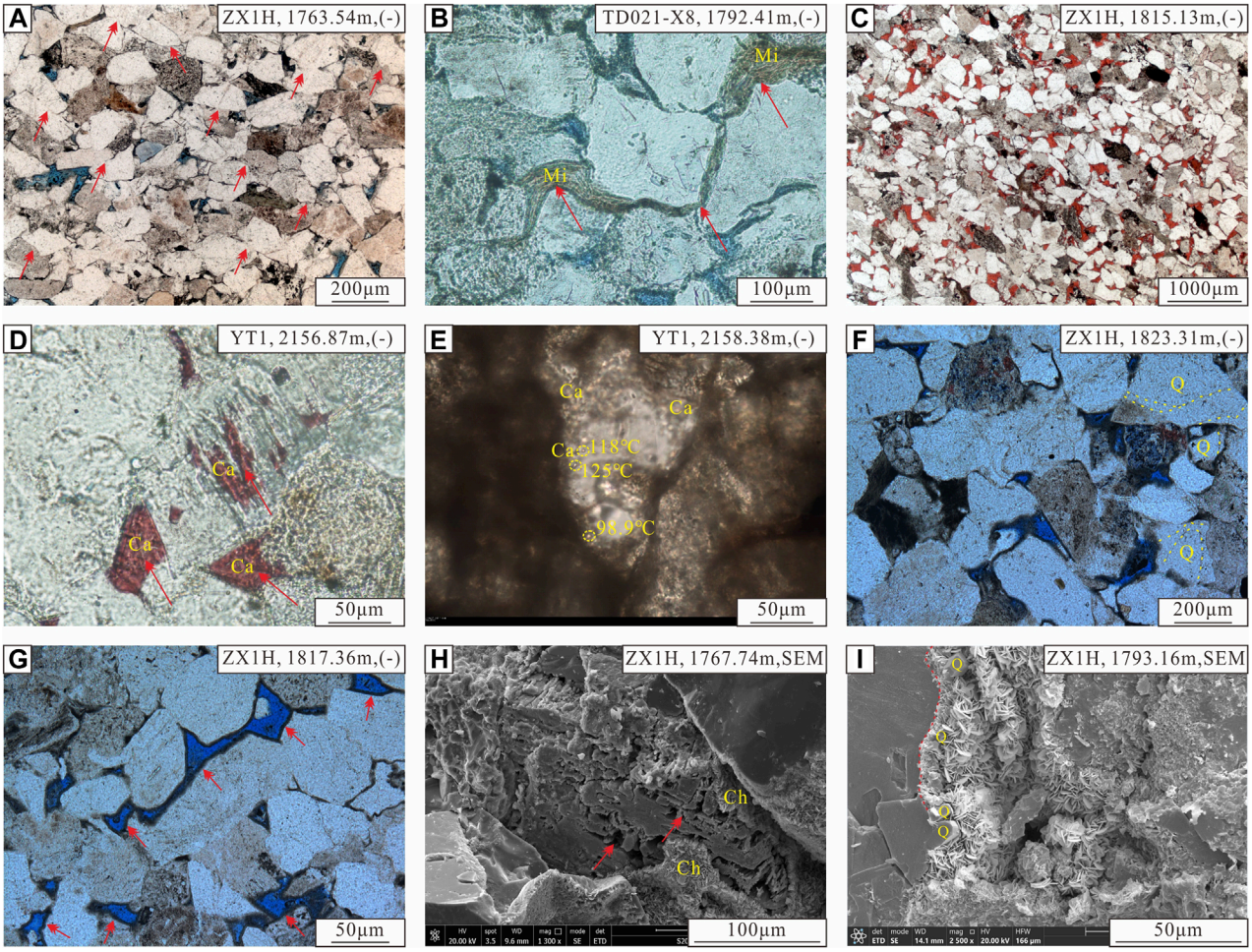

FIGURE 7
Diagenetic characteristics of the J_1l tight sandstones in the eastern Sichuan Basin. **(A)** Well ZX1H, 1763.54 m, J_1l^s segment, linear and concavo–convex contact relationship between particles; **(B)** well TD021-X8, 1792.41 m, J_1l^s segment, mica deformation under compression; **(C)** well ZX1H, 1815.13 m, J_1l^s segment, strong calcite cementation; **(D)** well YT1, 2156.87 m, J_1l^s segment, calcite cement-filled dissolution pores; **(E)** well YT1, 2,158.38 m, J_1l^s segment, fluid inclusion temperature of calcite cement; **(F)** well ZX1H, 1823.31 m, J_1l^s segment, two stages of siliceous cementation; **(G)** well ZX1H, 1817.36 m, J_1l^s segment, chlorite coatings associated with intergranular pores; **(H)** well ZX1H, 1767.74 m, J_1l^s segment, feldspar dissolution wrapped in chlorite coatings; and **(I)** well ZX1H, 1793.16 m, J_1l^s segment, siliceous nodules growing on chlorite flakes.

TABLE 2 Classification criteria for diagenetic intensity of the J_1l tight sandstones in the eastern Sichuan Basin [modified from Yang et al. (2014), Peng et al. (2016), and Liu et al. (2023)].

Diagenetic intensity	Compaction			Cementation		Dissolution	
	R_{co} (%)	CI	Particle contact relationship	R_{ce} (%)	Cementation type	R_d (%)	Pore type
Strong	≥70	≥2.5	Linear and concavo–convex contact	≥70	Basal and porous cementation	≥60	Intragranular dissolution pores Interparticle dissolution pores Mold pores
Medium	30–70	1.5–2.5	Point-line contact	30–70	Contact cementation	30–60	Small-diameter dissolution pores
Weak	≤30	≤1.5	Point contact	≤30	Mosaic cementation	≤30	Scattered dissolution pores

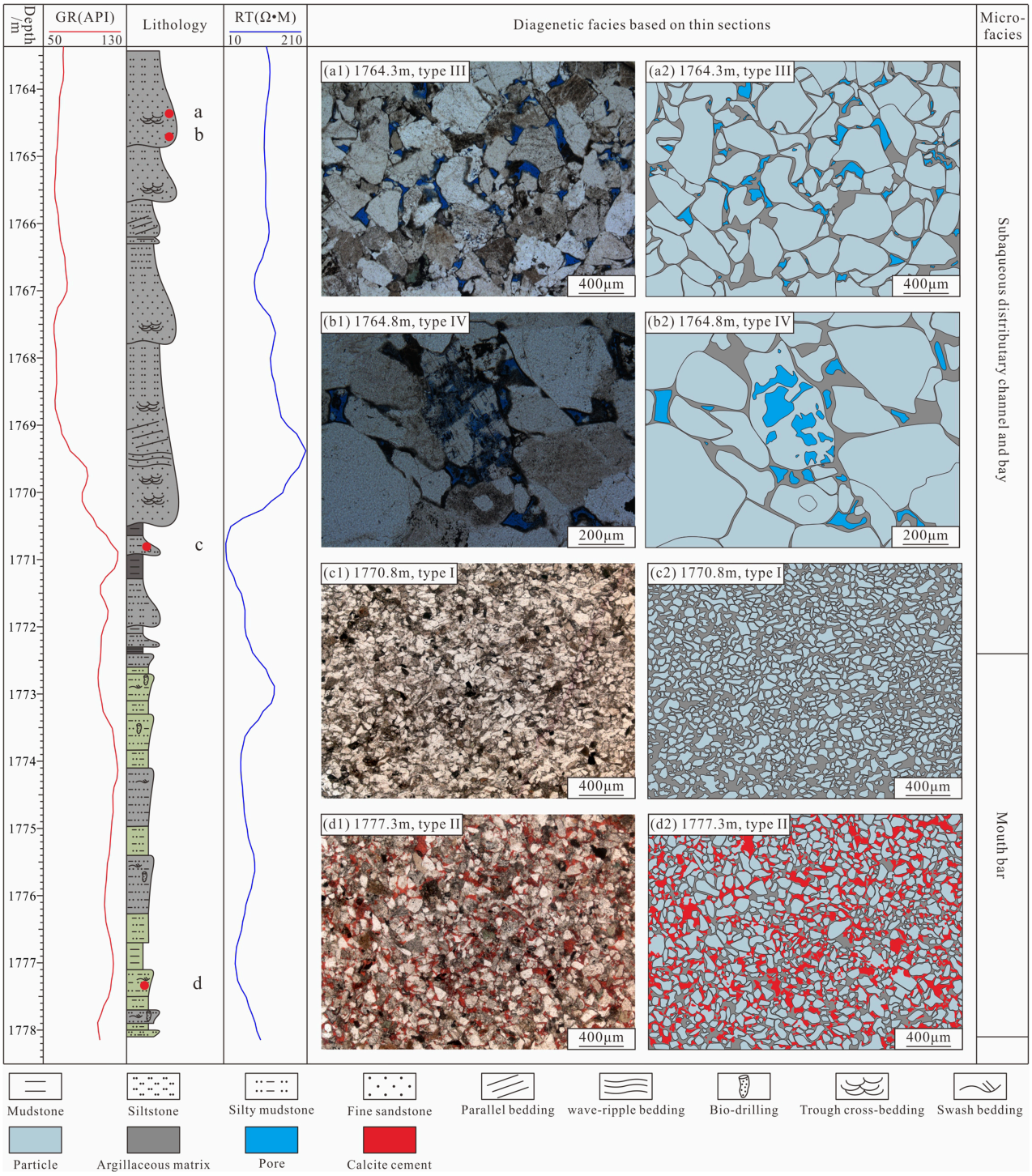

FIGURE 8
Sedimentological and diagenetic facies of the J_1l tight sandstones in Well ZX1H, eastern Sichuan Basin. Type I, strong compaction facies; type II, strong cementation facies; type III, chlorite-coating and intergranular pore facies; and type IV, weak dissolution and intragranular facies.

concavo–convex contact particles, and "d" represents the number of samples with stylolite contact particles.

$$\Phi_o = 20.91 + \frac{22.9}{S_0}, \tag{2}$$

$$R_{co} = \frac{\Phi_o\text{-}\Phi_r\text{-}V_c\text{-}V_m}{\Phi_0} \times 100\%, \tag{3}$$

$$R_{ce} = \frac{V_c}{V_c + \Phi_r} \times 100\%, \tag{4}$$

TABLE 3 Identification standards for sedimentological and diagenetic facies of the J_1l tight sandstones in the eastern Sichuan Basin.

Diagenetic facies		Sedimentary micro-facies	Lithology	Thin-section characteristic				Φ (%)	Well-logging response				
				R_{co} (%)	R_{ce} (%)	R_d (%)	P_d (%)		GR (API)	AC (μs/m)	RT (Ω•m)	DEN (g/cm^3)	CNL (%)
I	Strong compaction facies	MB and SS	Siltstone and argillaceous siltstone	78.6(12) 73.2-85.4	19.6(12) 14.6-26.8	0	0	1.42(12) 0.51-3.06	100.9(12) 63.6-116.8	64.8(12) 60.0-68.5	101.1(12) 55.4-260.8	2.65(12) 2.49-2.69	17.4(12) 10.8-22.4
II	Strong cementation facies	MB, SS, and edge of SDC	Various sandstones	37.6(9) 31.3-52.5	72.3(9) 67.5-78.7	0	0	1.84(9) 0.53-4.12	104.7(9) 97.1-114.5	64.1(9) 58.4-68.6	445.4(9) 59.6-1420.7	2.65(9) 2.63-2.70	14.5(9) 8.0-21.3
III	Chlorite-coating and intergranular pore facies	Middle of SDC and top of MB	Fine sandstone and siltstone	47.2(12) 27.8-59.3	13.8(12) 9.3-17.2	15.4(12) 13.2-17.6	31.8(12) 27.5-39.7	5.95(12) 1.74-7.97	68.3(12) 55.0-79.6	68.7(12) 60.1-80.8	76.2(12) 18.3-117.6	2.52(12) 2.43-2.60	15.4(12) 9.5-24.5
IV	Weak dissolution and intragranular pore facies	Middle of SDC and top of MB	Fine sandstone and siltstone	51.8(9) 39.2-76.3	23.4(9) 14.6-31.4	26.9(9) 16.5-28.8	57.4(9) 47.2-63.9	7.05(9) 5.53-8.35	68.2(9) 60.6-74.7	67.2(9) 64.0-70.4	92.8(9) 66.6-132.1	2.51(9) 2.44-2.61	16.3(9) 6.0-27.7
V	Medium compaction and cementation facies	Top and bottom of SDC	Fine sandstone and siltstone	56.7(21) 17.3-66.4	42.1(21) 30.7-54.8	9.5(21) 8.1-12.4	24.7(21) 18.8-29.5	3.75(21) 1.96-7.40	82.7(21) 65.5-100.6	65.0(21) 61.2-69.8	122.1(21) 38.1-335.3	2.59(21) 2.48-2.73	15.4(21) 6.4-34.3

Data in Table 3 can be expressed as $\frac{\text{Average value (Sample quantity)}}{\text{Minimum value–Maximum value}}$.

10.3389/feart.2024.1441548

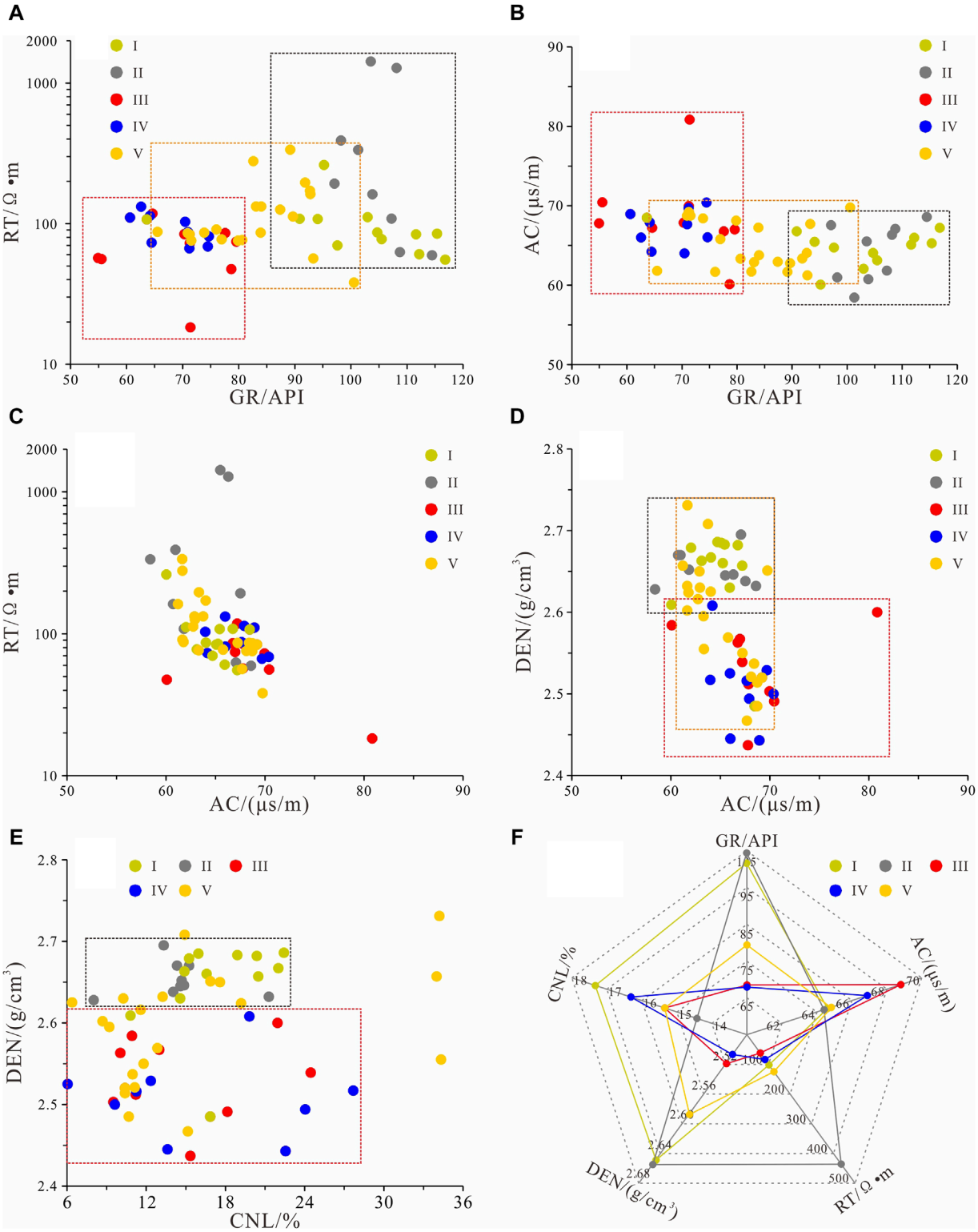

FIGURE 9
Well-logging parameter crossplots of the J_1l diagenetic facies in the eastern Sichuan Basin. I: Strong compaction facies; II: Strong cementation facies; III: Chlorite coating and intergranular pore facies; IV: Weak dissolution and intragranular facies; V: Medium compaction and cementation facies. **(A)**: The Interaction diagram between GR and RT; **(B)**: The Interaction diagram between GR and AC; **(C)**: The Interaction diagram between AC and RT; **(D)**: The Interaction diagram between AC and DEN; **(E)**: The Interaction diagram between CNL and DEN; **(F)**: The radar chart among GR, AC, RT, DEN, CNL.

$$R_d = \frac{P_d}{P_a} \times 100\%, \quad (5)$$

where Φ_o and Φ_r indicate the original porosity and current residual intergranular porosity, respectively, the unit is %; S_o is the sorting coefficient, dimensionless; R_{co}, R_{ce}, and R_d represent the apparent compaction rate, apparent cementation rate, and apparent dissolution rate, respectively, all in percentage (%); V_c and V_m refer to the volume fractions of diagenetic cements and micropores in the argillaceous matrix, %; and P_d and P_a stand for the plane porosity of secondary dissolution pores, all pores in percentage (%). These parameters are estimated through quantitative statistics of casting thin sections under the microscope.

Based on the sedimentary micro-facies and anatomy of sand bodies, and considering the relative intensities of various diagenesis and predominant types of micro-pores, a composite nomenclature is adopted in this study, using "sedimentary micro-facies (sand body parts) + typical diagenetic events + predominant pore types." Five diagenetic facies, including strong compaction facies (type I), strong cementation facies (type II), chlorite-coating and intergranular pore facies (type III), weak dissolution and intragranular facies (type IV), and medium compaction and cementation facies (type V) have been identified (Figure 8; Table 3). Metasomatism is common, but its impact on reservoir quality is limited, so no further discussion will be conducted here.

In well ZX1H, the strong compaction facies (type I) and strong cementation facies (type II) are mainly distributed in MB and SS with the finer particle size and higher content of the argillaceous matrix, as well as along the edges of SDC, which are characterized by the high R_{co} value of 73.2%–85.4% (av. 78.6%) and the R_{ce} value of 67.5%–78.7% (av. 72.3%), respectively. Simultaneously, there is almost no secondary dissolution, and R_d and P_d values are close to zero (Figure 8; Table 3). The chlorite-coating facies and weak dissolution facies improve the reservoir quality by protecting the primary intergranular pores or increasing the secondary intragranular pores (Figure 8), with the average porosities of 5.95 and 7.05 significantly higher than 1.42 and 1.84 of type I and type II diagenetic facies (Table 3). The R_{co} and R_{ce} parameters indicate that both of them are characterized by moderate compaction and weak cementation diagenesis, whereas R_d and P_d reveal varying degrees of dissolution (Table 3). It is clear that type III and type IV diagenetic facies in the middle of SDC and the top of MB are indicators for finding favorable reservoirs in the study area (Figure 8). The medium compaction and cementation facies (type V) are common in siltstones and fine sandstones at the top and bottom of SDC, resulting in porosity ranging from 1.96% to 7.40%, with an average value of 3.75% (Table 3).

5.2 Well-logging responses of sedimentological and diagenetic facies

When the matrix minerals of rocks, that is, the sedimentary facies, are essentially determined, the differences in diagenetic characteristics, pore structures, and physical properties of various diagenetic facies lead to their different responses on well-logging data. On the basis of deep repositioning of core samples and standardization of well-logging curves, the longitudinal continuous identification of diagenetic facies can be achieved by summarizing the well-logging response patterns of different diagenetic facies (Peng et al., 2016; Lai Jet al., 2018; Liu AQ. et al., 2023). Natural gamma (GR) ray well logging can reflect the sedimentary environment and lithology, and density (DEN), interval transit time (AC), and neutron porosity (CNL) well logging are intuitive displays of reservoir physical properties, whereas resistivity well logging can indirectly reflect the pore structures of reservoirs (Cao et al., 2015; Huang et al., 2022). Therefore, according to the correlation among GR, AC, RT, DEN, CNL, and diagenetic facies, well-logging identification standards for diagenetic facies have been established (Figure 9; Table 3).

First, by intersecting GR with RT and AC, respectively, the constructive type III and type IV diagenetic facies can be clearly distinguished from the destructive type I and type II diagenetic facies, whereas the transitional type V intersects with both of them (Figures 9A, B). Affected by strong compaction and relatively high content of argillaceous matrix, type I diagenetic facies is characterized by high amplitude GR in the range of 63.6–116.8 API (av. 100.9 API) and medium amplitude RT in the range of 55.4–260.8 Ω•m (av. 101.1 Ω•m) (Table 3). After being strongly cemented by calcite, the reservoir porosity decreases, and the rock density increases, resulting in "three high and two low" well-logging responses of type II diagenetic facies, that is, high RT (59.6–1420.7 Ω•m, av. 445.4 Ω•m), high DEN (2.63–2.70 g/cm^3, av. 2.65 g/cm^3), high GR (97.1–114.5 API, av. 104.7 API), low CNL (8.0%–21.3%, av. 14.5%), and low AC (58.4–68.6 μs/m, av. 64.1 μs/m) (Figures 9A–E; Table 3). On the contrary, the development of chlorite coatings is beneficial for maintaining porosity, as evidenced in well-logging data by low GR (55.0–79.6 API, av. 68.3 API), low RT (18.3–117.6 Ω•m, av. 76.2 Ω•m), low DEN (2.43–2.60 g/cm^3, av. 2.52 g/cm^3), and relatively high AC (60.1–80.8 μs/m, av. 68.7 μs/m), along with moderate CNL (9.5%–24.5%, av. 15.4%) as typical features (Figures 9A–E; Table 3). The well-logging responses of type IV diagenetic facies are essentially consistent with these, with only slight increases in RT and CNL, ranging from 66.6 Ω•m to 132.1 Ω•m (av. 92.8 Ω•m) and 6.0% to 27.7% (av. 16.3%), respectively (Table 3). The radar chart indicates that as favorable tight sandstone reservoirs, type III and type IV diagenetic facies can be identified by high AC and low GR, DEN, and RT, whereas the ineffective exploration targets of type I and type II diagenetic facies exhibit high GR, DEN, CNL, and RT (Figure 9F).

5.3 Machine learning method of sedimentological and diagenetic facies and its application

Machine learning can efficiently process large-scale geological data, including geophysical data and chemical properties of rock samples. In the processing, machine learning fully excavates well-logging information, automatically selects key parameter features related to sedimentological and diagenetic facies, and accelerates data decision-making behaviors, reducing subjectivity

TABLE 4 Machine learning models and prediction results of the J_1l diagenetic facies in the eastern Sichuan Basin.

Sample no.	AC (μs/m)	CAL (cm)	CNL (%)	DEN (g/cm^3)	GR (API)	RT (Ω•m)	RXO (Ω•m)	Label	
0	65.559	9.169	11.572	2.664	103.105	54.534	50.788	Type I	Strong compaction facies
1	66.381	9.820	13.498	2.604	124.422	39.383	36.643	Type I	Strong compaction facies
2	67.803	10.021	16.844	2.565	127.910	30.057	27.748	Type V	Medium compaction and cementation facies
3	67.629	9.849	24.650	2.541	120.058	23.508	21.481	Type III	Chlorite-coating and intergranular pore facies
4	67.205	9.708	25.402	2.543	111.427	24.251	22.053	Type IV	Weak dissolution and intragranular pore facies
…	…	…	…	…	…	…	…	…	…
9,806	67.778	9.493	14.675	2.396	82.379	20.178	21.717	Type II	Strong cementation facies
9,807	67.780	9.149	14.675	2.307	80.447	20.195	21.698	Type II	Strong cementation facies
9,808	67.809	7.805	14.583	2.256	78.224	20.261	21.729	Type III	Chlorite-coating and intergranular pore facies
9,809	67.780	6.788	14.824	2.238	79.169	20.390	21.849	Type III	Chlorite-coating and intergranular pore facies
9,810	67.787	6.310	14.751	2.246	82.098	20.397	21.918	Type III	Chlorite-coating and intergranular pore facies

and human errors (Zheng et al., 2021; Antariksa et al., 2022; Zhao et al., 2022; Gu et al., 2023; Hansen et al., 2023). The common prediction models include decision tree algorithm, random forest algorithm, and Bayesian algorithm (Zheng et al., 2021; Antariksa et al., 2022; Hansen et al., 2023). For the identification of diagenetic facies in logging, probabilistic neural network is used, and the simulated classification surface is close to the surface under the Bayesian optimal criterion.

On the basis of the mentioned sedimentological and diagenetic facies and their well-logging responses, CAL and RXO well-logging data are added to the well-logging database after standardization, serving as the input data for machine learning. In order to enhance the model's generalization ability, 70% of the data are randomly extracted as the training samples (Table 4). During the training process, the remaining 30% data are used as the validation dataset to test the recognition results of different well-logging combinations. As shown in Figure 10, five of the six thin sections from well TD021-X8 match the expected values, and the overall accuracy of the training results is around 75%, indicating that the training results are relatively reliable. The diagenetic facies of type III and type IV are mostly developed in the middle of thick subaqueous distributary channels (Figure 10), making them the preferred exploration targets for favorable reservoirs in lacustrine delta-front tight sandstones.

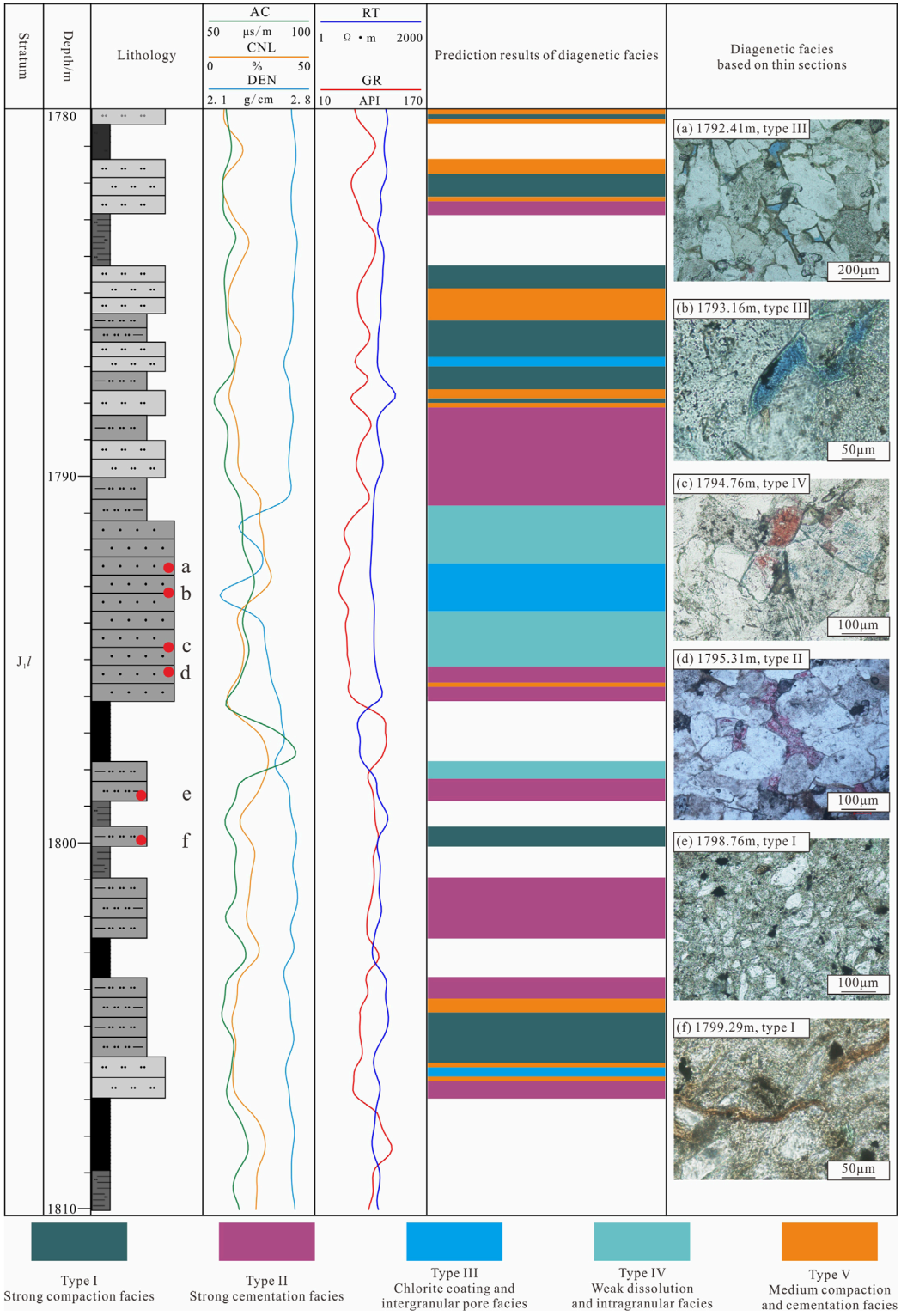

FIGURE 10
Machine learning results of the J_1l diagenetic facies in well TD021-X8, eastern Sichuan Basin.

6 Conclusion

Taking the J_1l delta-front tight sandstones in the eastern Sichuan Basin as a case, the types, characteristics, and well-logging responses of the main sedimentological and diagenetic facies were analyzed in detail, and the understanding was further applied to petroleum exploration by means of the machine learning method. The main conclusions are as follows.

(1) Under the warm and humid paleoclimate and lake transgression and regression cycles, J_1l develops lacustrine delta-front sub-facies, which are mainly characterized by subaqueous distributary channels and mouth bars.
(2) The J_1l sandstones exhibit typical dense features, with porosity and permeability in the range of 0.48%–11.24% (av. 3.87%) and 0.0003×10^{-3} μm^2–0.653×10^{-3} μm^2 (av. 0.026×10^{-3}μm^2), respectively, and the reservoir quality largely depends on the pore–throat content with radii greater than 0.006 μm. Strong compaction and cementation are the major diagenetic events leading to densification, whereas chlorite coatings and weak dissolution, as constructive diagenetic processes, retain some primary pores and increase a few dissolution pores.
(3) According to the types and development degree of sedimentary micro-facies, diagenesis, and pore–throats, five sedimentological and diagenetic facies have been identified in the J_1l tight sandstones, namely, strong compaction facies of MB and SS (type I); strong cementation facies of MB, SS, and the edge of SDC (type II); chlorite-coating and intergranular pore facies in the middle of SDC and the top of MB (type III); weak dissolution and intragranular facies in the middle of SDC and the top of MB (type IV); and medium compaction and cementation facies at the top and bottom of SDC (type V).
(4) The sedimentological and diagenetic facies of type III and type IV are favorable tight sandstone reservoirs in lacustrine delta-front, characterized by high AC and low GR, DEN, and RT in well logging. On the basis of the sedimentological and diagenetic facies and their well-logging responses, CAL and RXO well-logging data are added to the well-logging database after standardization, serving as the input data for machine learning. In addition, the training results are relatively reliable. The thick-layer, coarse-grained subaqueous distributary channels, in which the diagenetic facies of type III and type IV are mostly developed, have been identified as the primary exploration targets for tight hydrocarbon reservoirs.

Data availability statement

The original contributions presented in the study are included in the article material; further inquiries can be directed to the corresponding author.

Author contributions

CY: data curation, investigation, software, and writing–original draft. WG: data curation, investigation, methodology, software, and writing–original draft. LC: conceptualization, funding acquisition, resources, supervision, validation, visualization, writing–original draft, writing–review and editing, data curation, and methodology. YZ: formal analysis, funding acquisition, project administration, supervision, validation, and writing–review and editing. ZZ: formal analysis, funding acquisition, project administration, resources, validation, and writing–review and editing. YL: methodology, software, supervision, validation, and writing–original draft. TY: conceptualization, methodology, supervision, validation, and writing–review and editing.

Funding

The authors declare that financial support was received for the research, authorship, and/or publication of this article. This work was co-supported by the National Natural Science Foundation of China (Nos 41906188 and 42372139) and the Science and Technology Program of Sichuan Province (Nos 2022NSFSC0990 and 2023NSFSC1986).

Acknowledgments

The authors would like to appreciate PetroChina Southwest Oil and Gas Field Company for providing rock samples and partial testing data.

Conflict of interest

Author YZ was employed by PetroChina Changqing Oilfield Company.

The remaining authors declare that the research was conducted in the absence of any commercial or financial relationships that could be construed as a potential conflict of interest.

Publisher's note

References

Alam, K., Abdullatif, O., El-Husseiny, A., and Babalola, L. (2022). Depositional and diagenetic controls on reservoir heterogeneity and quality of the Bhuban formation, Neogene Surma Group, Srikail Gas Field, Bengal Basin, Bangladesh. *J. Asian Earth Sci.* 223. doi:10.1016/j.10.1016/J.JSEAES.2021.104985

Antariksa, G., Muammar, R., and Lee, J. (2022). Performance evaluation of machine learning-based classification with rock-physics analysis of geological lithofacies in Tarakan Basin, Indonesia. *J. Petroleum Sci. Eng.* 208, 109250. doi:10.1016/j.petrol.2021.109250

Bahrehvar, M., Mehrabi, H., Akbarzadeh, S., and Rahimpour-Bonab, H. (2021). Depositional and diagenetic controls on reservoir quality of the uppermost Jurassic-Lower Cretaceous sequences in the Persian Gulf; a focus on J–K boundary. *J. Petroleum Sci. Eng.* 201, 108512. doi:10.1016/j.petrol.2021.108512

Beard, D. C., and Weyl, P. K. (1973). Influence of texture on porosity and permeability of unconsolidated sand. *AAPG Bull.* 57 (2), 349–369. doi:10.1306/819a4272-16c5-11d7-8645000102c1865d

Beckmann, B., Flögel, S., Hofmann, P., Schulz, M., and Wagner, T. (2005). Orbital forcing of cretaceous river discharge in tropical africa and ocean response. *Nature* 437, 241–244. doi:10.1038/nature03976

Bloch, S., Lander, R. H., and Bonnell, L. (2002). Anomalously high porosity and permeability in deeply buried sandstone reservoirs: origin and predictability. *AAPG Bull.* 86 (2), 301–328. doi:10.1306/61eedabc-173e-11d7-8645000102c1865d

Cai, L. X., Guo, X. W., Zhang, X. H., Zeng, Z., Xiao, G., Pang, Y., et al. (2019). Pore-throat structures of the permian longtan formation tight sandstones in the South yellow sea basin, China: a case study from borehole CSDP-2. *J. Petroleum Sci. Eng.* 186, 106733. doi:10.1016/j.petrol.2019.106733

Cai, L. X., Zhang, X. H., Guo, X. W., Gao, X. H., Pang, Y. M., and Zhu, X. Q. (2023). Formation mechanisms and geological significance of the lower triassic fine-grained mixed sedimentary rocks in the central uplift of the South yellow sea basin, eastern China. *J. Asian Earth Sci.* 247, 105609. doi:10.1016/j.jseaes.2023.105609

Cao, Y. C., Xi, K. L., Zhao, X. Z., Jin, F. M., Zhou, L., Su, R., et al. (2015). Reservoir diagenetic facies and its logging identification of Es4s in Langgu sag. *J. Central South Univ. Sci. Technol.* 46 (11), 4183–4194. (in Chinese with English abstract).

Carvalho, M. V. F., De Ros, L. F., and Gomes, N. S. (1995). Carbonate cementation patterns and diagenetic reservoir facies in the Campos Basin Cretaceous turbidites, offshore eastern Brazil. *Mar. Petroleum Geol.* 12 (7), 741–758. doi:10.1016/0264-8172(95)93599-y

Chen, Y. H., and Liu, Y. (1994). Diagenetic facies — a new approach to the prediction of reservoir rocks. *Exp. Pet. Geol.* 16 (3), 274–281. (in Chinese with English abstract).

Cheng, D. W., Zhang, Z. J., Hong, H. T., Zhang, S., Qin, C., Yuan, X., et al. (2023a). Sequence structure, sedimentary evolution and their controlling factors of the jurassic Lianggaoshan Formation in the east Sichuan Basin, SW China. *Petroleum Explor. Dev.* 50 (2), 293–305. doi:10.1016/s1876-3804(23)60388-x

Cheng, D. W., Zhang, Z. J., Hong, H. T., Zhang, S., Qin, C., Yuan, X., et al. (2023b). Sequence structure, sedimentary evolution and their controlling factors of the jurassic Lianggaoshan Formation in the east Sichuan Basin, SW China. *Petroleum Explor. Dev.* 50, 293–305. doi:10.1016/s1876-3804(23)60388-x

Cho, M. S., and Fawcett, J. J. (1986). Morphologies and growth mechanisms of synthetic mg-chlorite and cordierite. *Am. Mineralogist* 71 (1-2), 78–84.

Cui, Y. F., Wang, G. W., Jones, S. J., Zhou, Z., Ran, Y., Lai, J., et al. (2017). Prediction of diagenetic facies using well logs — a case study from the upper Triassic Yanchang Formation, Ordos Basin, China. *Mar. Petroleum Geol.* 81, 50–65. doi:10.1016/j.marpetgeo.2017.01.001

Dai, J. X., Ni, Y. Y., Liu, Q. Y., Wu, X., Gong, D., Hong, F., et al. (2021). Sichuan super gas basin in southwest China. *Petroleum Explor. Dev.* 48 (6), 1251–1259. doi:10.1016/s1876-3804(21)60284-7

Dill, H. G., Khishigsuren, S., Melcher, F., Bulgamaa, J., Bolorma, K., Botz, R., et al. (2005). Facies-related diagenetic alteration in lacustrine-deltaic red beds of the paleogene ergeliin zoo formation (erdene sum area, S. Gobi, Mongolia). *Sediment. Geol.* 181, 1–24. doi:10.1016/j.sedgeo.2005.06.007

Ehrenberg, S. N. (1993). Preservation of anomalously high porosity in deeply buried sandstones by grain-coating chlorite: examples from the Norwegian continental shelf. *AAPG Bull.* 77 (7), 1260–1286. doi:10.1306/bdff8e5c-1718-11d7-8645000102c1865d

Fang, W. X. (2020). Classification and types of diagenetic lithofacies systems in the sedimentary basin. *Geol. Bull. China* 39 (11), 1692–1714. (in Chinese with English abstract).

Greber, N. D., and Dauphas, N. (2019). *The chemistry of fine-grained terrigenous sediments reveals a chemically evolved Paleoarchean emerged crust*, 255, 247–264.

Gu, Y. F., Li, Y., Yang, Y. S., Xiao, B., Zhang, D., and Bao, Z. (2023). Classification pattern of lacustrine carbonate diagenetic facies and logging-based data-driven prediction via a generalized and robust ensemble learning: a demonstration of pre-salt profile, santos basin. *Geoenergy Sci. Eng.* 223, 211543. doi:10.1016/j.geoen.2023.211543

Guo, J. Y., Qi, X. N., Hou, L. H., Hao, A., Zeng, X., Lin, S., et al. (2022). Origin and accumulation models of ultra-low permeability-tight sandstone (gravel) gas in Bohai Bay Basin, China. *J. Nat. Gas Geoscience* 7, 211–223. doi:10.1016/j.jnggs.2022.08.002

Haile, B. G., Klausen, T. G., Czarniecka, U., Xi, K., Jahren, J., Hellevang, H., et al. (2017). How are diagenesis and reservoir quality linked to depositional facies? A deltaic succession, Edgeøya, Svalbard. *Mar. Pet. Geol.* 92, 519–546. doi:10.1016/j.marpetgeo.2017.11.019

Han, Z., Hu, X. M., Hu, Z. Y., Jenkyns, H. C., and Su, T. (2022). Geochemical evidence from the Kioto Carbonate Platform (Tibet) reveals enhanced terrigenous input and deoxygenation during the early Toarcian. *Glob. Planet. Change* 215, 103887. doi:10.1016/j.gloplacha.2022.103887

Hansen, H. N., Haile, B. G., Müller, R., and Jahren, J. (2023). New direction for regional reservoir quality prediction using machine learning - example from the Stø Formation, SW Barents Sea, Norway. *J. Petroleum Sci. Eng.* 220, 111149. doi:10.1016/j.petrol.2022.111149

He, D. F. (2022). Multi-cycle superimposed sedimentary basins in China: formation, evolution, geologic framework and hydrocarbon occurrence. *Earth Sci. Front. (in Chinese with English abstract)* 29 (6), 24–59. doi:10.13745/j.esf.sf.2022.8.1

He, Z., Shi, J. A., Tang, Y., Ding, C., and Zhang, S. C. (2011). Characteristics of diagenesis and diagenetic facies of permian clastic reservoir in northwest margin of junggar basin. *Acta Sedimentologica Sinica (in Chinese with English abstract)* 29 (6), 1069–1078. doi:10.14027/j.cnki.cjxb.2011.06.003

Henares, S., Caracciolo, L., Cultrone, G., Fernández, J., and Viseras, C. (2014). The role of diagenesis and depositional facies on pore system evolution in a Triassic outcrop analogue (SE Spain). *Marine and Petroleum Geology* 51, 136–151. doi:10.1016/j.marpetgeo.2013.12.004

Huang, H. Y., He, D. F., Li, Y. Q., and Zhang, C. (2023). Provenance and paleogeography of the Early Paleozoic basin in the northern Yangtze Block: constraints from detrital zircon U-Pb-Hf data. *Gondwana Research* 125, 210–228. doi:10.1016/j.gr.2023.08.011

Huang, L. S., Yan, J. P., Liu, M. J., Zhang, Z., Ye, S. J., Zhang, F., et al. (2022). Diagenetic facies logging identification and application of deep tight sandstone gas reservoir: a case study of the third member of Xujiahe formation in Dayi area of western Sichuan depression. *Journal of China University of Mining & Technology* 51 (1), 107–123. (in Chinese with English abstract). doi:10.13247/j.cnki.jcumt.001325

Huang, X., Duan, D. P., Liu, B. B., Li, B. Y., Ding, F., Wang, W., et al. (2021). Origin mechanism of chlorite and its impact on reservoir properties in Huagang Formation, Xihua Depression. *Journal of Jilin University* 51 (3), 669–679. (Earth Science Edition) (in Chinese with English abstract). doi:10.13278/j.cnki.jjuese.20200149

Jia, C. Z., Pang, X. Q., and Song, Y. (2023). Whole petroleum system and ordered distribution pattern of conventional and unconventional oil and gas reservoirs. *Petroleum Science* 20, 1–19. doi:10.1016/j.petsci.2022.12.012

Jia, C. Z., Zou, C. N., Yang, Z., Zhu, R., Chen, Z., Zhang, B., et al. (2018). Significant progress of continental petroleum geological theory in basins of Central and Western China. *Petroleum Exploration and Development* 45 (4), 573–588. doi:10.1016/s1876-3804(18)30064-8

Jones, B., and Manning, D. A. C. (1994). Comparison of geochemical indices used for the interpretation of palaeoredox conditions in ancient mudstones. *Chemical Geology* 111, 111–129. doi:10.1016/0009-2541(94)90085-x

Kane, O. I., Hu, M. Y., Cai, Q. S., Deng, Q., Yang, W., and Zuo, M. (2023). Sedimentary facies, lithofacies paleogeography, and an evaluation of the Ordovician sequences in the Sichuan Basin, southwest China. *Marine and Petroleum Geology* 149, 106096. doi:10.1016/j.marpetgeo.2023.106096

Khalifa, M. A., and Morad, S. (2015). Impact of depositional facies on the distribution of diagenetic alterations in the Devonian shoreface sandstone reservoirs, Southern Ghadamis Basin, Libya. *Sedimentary Geology* 329, 62–80. doi:10.1016/j.sedgeo.2015.09.003

Korsch, R. J., Mai, H. Z., Sun, Z. C., and Gorter, J. (1991). The Sichuan Basin, southwest China: a late proterozoic (sinian) petroleum province. *Precambrian Research* 54, 45–63. doi:10.1016/0301-9268(91)90068-l

Kra, K., Qiu, L. W., Yang, Y. Q., Yang, B. L., Ahmed, K. S., Camara, M., et al. (2022). Sedimentological and diagenetic impacts on sublacustrine fan sandy conglomerates reservoir quality: An example of the Paleogene Shahejie Formation (Es4s Member) in the Dongying Depression, Bohai Bay Basin (East China). *Sediment. Geol.* 427. doi:10.1016/J.SEDGEO.2021.106047

Külaots, I., Goldfarb, J. L., and Suuberg, E. M. (2010). Characterization of Chinese, American and Estonian oil shale semicokes and their sorptive potential. *Fuel* 89, 3300–3306. doi:10.1016/j.fuel.2010.05.025

Lai, J., Fan, X. C., Pang, X. J., Zhang, X., Xiao, C., Zhao, X., et al. (2019). Correlating diagenetic facies with well logs (conventional and image) in sandstones: the Eocene-Oligocene Suweiyi Formation in Dina 2 Gasfield, Kuqa depression of China. *Journal of Petroleum Science and Engineering* 174, 617–636. doi:10.1016/j.petrol.2018.11.061

Lai, J., Fan, X. C., Liu, B. C., Pang, X. J., Zhu, S. F., Xie, W. B., et al. (2020). Qualitative and quantitative prediction of diagenetic facies via well logs. *Mar. Pet. Geol.* 120, 104486. doi:10.1016/j.marpetgeo.2020.104486

Lai, J., Wang, G. W., Wang, S., Cao, J., Li, M., Pang, X., et al. (2018). Review of diagenetic facies in tight sandstones: diagenesis, diagenetic minerals, and prediction via well logs. *Earth-Science Reviews* 185, 234–258. doi:10.1016/j.earscirev.2018.06.009

Lai, J., Xiao, L., Zhao, X., Zhao, F., Li, Y. H., Zhu, S. F., et al. (2023). Genesis and logging evaluation of deep to ultra-deep high-quality clastic reservoirs: a case study of the Cretaceous Bashijiqike Formation in Kuqa depression. *Acta Petrolei Sinica (in Chinese with English abstract)* 44 (4), 612–625.

Law, B. E., and Curtis, J. B. (2002). Introduction to unconventional petroleum systems. *American Association of Petroleum Geologists Bulletin* 86 (11), 1851–1852. doi:10.1306/61eedda0-173e-11d7-8645000102c1865d

Li, S. M., Han, R. B., Du, Y. J., Liu, P., and Bie, H. (2020). Quantitative characterization of diagenetic reservoir facies of the Karamay alluvial fan in the Junggar Basin, western China. *Journal of Petroleum Science and Engineering* 188, 106921. doi:10.1016/j.petrol.2020.106921

Li, Y. Q., He, D. F., Li, D., Lu, R., Fan, C., Sun, Y., et al. (2018). Sedimentary provenance constraints on the jurassic to cretaceous paleogeography of Sichuan Basin, SW China. *Gondwana Research* 60, 15–33. doi:10.1016/j.gr.2018.03.015

Li, Z. H., Zhang, L. Q., Yuan, W. F., Chen, X., and Li, M. (2022). Logging identification for diagenetic facies of tight sandstone reservoirs: a case study in the lower jurassic ahe formation, kuqa depression of tarim basin. *Marine and Petroleum Geology* 139, 105601. doi:10.1016/j.marpetgeo.2022.105601

Liu, A. Q., Tian, J. C., Chen, S. C., Yi, J. Z., Zhang, S. M., Luo, X., et al. (2023a). Characteristics and controlling factors of Jurassic Lianggaoshan Formation tight sandstone reservoirs in the eastern Sichuan Basin. *Mineralogy and Petrology (in Chinese with English abstract)* 43 (1), 144–155. doi:10.19719/j.cnki.1001-6872.2023.01.12

Liu, H. K., Ai, Y., Wang, G. W., Chen, K. J., Cai, D. Y., Cao, J. T., et al. (2023b). Quantitative well logging evaluation of diagenetic facies of deep and ultra deep tight sandstone reservoirs: a case study of Bozi-Dabei area in Kuqa Depression. *Bulletin of Geological Science and Technology (in Chinese with English abstract)* 42 (1), 299–310. doi:10.19509/j.cnki.dzkq.2022.0256

Liu, Y. F., Hu, W. X., Cao, J., Wang, X., Tang, Q., Wu, H., et al. (2018). Diagenetic constraints on the heterogeneity of tight sandstone reservoirs: a case study on the Upper Triassic Xujiahe Formation in the Sichuan Basin, southwest China. *Marine and Petroleum Geology* 92, 650–669. doi:10.1016/j.marpetgeo.2017.11.027

Meng, L. F., Chen, W., Shen, T., and Cai, J. (2022). A study on the provenance of early to late Triassic clastic rocks from the northwestern Sichuan Basin, southwestern China: constraints on the early Mesozoic tectonic evolution of the western Yangtze Block. *Frontiers in Earth Science* 10, 940301. doi:10.3389/feart.2022.940301

Moradia, A. V., Sarı, A., and Akkayaa, P. (2016). Geochemistry of the miocene oil shale (hançili formation) in the çankırı-çorum basin, Central Turkey: implications for paleoclimate conditions, source–area weathering, provenance and tectonic setting. *Sedimentary Geology* 341, 289–303. doi:10.1016/j.sedgeo.2016.05.002

Mou, C. L., Wang, X. P., Wang, Q. Y., and Wang, Y. C. (2016). The recognition of diagenetic facies on the case from the reservoir in He8 section of Shihezi Formation, East II part of Sulige gas field, Qrdos Basin. *Acta Sedimentologica Sinica (in Chinese with English abstract)* 34 (2), 346–355. doi:10.14027/j.cnki.cjxb.2016.02.013

Mou, W. W., Wang, Q., Tian, B., He, L. W., and Hu, Z. J. (2017). The diagenetic facies logging response characteristics of medium-deep reservoirs in the north slope of Baiyun Sag, Pearl River Mouth Basin. *Natural Gas Geoscience (in Chinese with English abstract)* 28 (10), 1601–1612.

Packham, G. H., and Keith, A. W. C. (1960). The principle of diagenetic facies and some of its implications. *The Journal of Geology* 68 (4), 392–407. doi:10.1086/626673

Peng, J., Wu, H. M., Han, H. D., Yang, S. J., Zhang, H. B., and Liu, L. (2016). Study on diagenetic facies of the Donghetang tight sandstone reservoirs in Bachu area. *Oil & Gas Geology (in Chinese with English abstract)* 37 (2), 245–255.

Railsback, L. B. (1984). Carbonate diagenetic facies in the upper pennsylvanian dennis formation in Iowa, Missouri, and Kansas. *Journal of Sedimentary Research* 54 (3), 986–999. doi:10.1306/212f8549-2b24-11d7-8648000102c1865d

Şengör, A. M. C. (1985). Geology: east asian tectonic collage. *Nature* 318, 16–17. doi:10.1038/318016a0

Soeder, D. J. (2018). The successful development of gas and oil resources from shales in North America. *Journal of Petroleum Science and Engineering* 163, 399–420. doi:10.1016/j.petrol.2017.12.084

Stephen, A. H. (2006). Tight gas sands. *SPE Journal* 58 (6), 86–93. doi:10.2118/103356-jpt

Sun, L. D., Zou, C. N., Jia, A. L., Wei, Y., Zhu, R., Wu, S., et al. (2019). Development characteristics and orientation of tight oil and gas in China. *Petroleum Exploration and Development* 46 (6), 1073–1087. doi:10.1016/s1876-3804(19)60264-8

Wang, C. Y., Chang, J., Li, N., Hong, H. T., Li, Y. N., Wang, X. J., et al. (2022a). Paleo-water-depth reconstruction of early Jurassic lakes in the eastern Sichuan Basin. *Acta Sedimentologica Sinica*. (in Chinese with English abstract). doi:10.14027/j.issn.1000-0550.2022.036

Wang, J., Cao, Y. C., Liu, K. Y., Liu, J., and Kashif, M. (2017). Identification of sedimentary-diagenetic facies and reservoir porosity and permeability prediction: an example from the Eocene beach-bar sandstone in the Dongying Depression, China. *Marine and Petroleum Geology* 82, 69–84. doi:10.1016/j.marpetgeo.2017.02.004

Wang, X. J., Hong, H. T., Wu, C. J., Liu, M., Guan, X., Chen, S. L., et al. (2022b). Characteristics and formation mechanisms of tight sandstone reservoirs in Jurassic Shaximiao Formation, central of Sichuan Basin. *Journal of Jilin University (Earth Science Edition)* 52 (4), 1037–1051. (in Chinese with English abstract). doi:10.13278/j.cnki.jjuese.20210247

Wang, Z. C., Jiang, H., Chen, Z. Y., Liu, J., Ma, K., Li, W., et al. (2020). Tectonic paleogeography of Late Sinian and its significances for petroleum exploration in the middle-upper Yangtze region, South China. *Petroleum Exploration and Development* 47 (5), 946–961. doi:10.1016/s1876-3804(20)60108-2

Wang, Z. C., Shi, Y. Z., Wen, L., Jiang, H., Jiang, Q., Huang, S., et al. (2022c). Exploring the potential of oil and gas resources in Sichuan Basin with super basin thinking. *Petroleum Exploration and Development* 49 (5), 977–990. doi:10.1016/s1876-3804(22)60326-4

Wang, Z. Y., Zhou, N. W., Lu, S. F., Liu, Y., Lin, L., Liu, Y., et al. (2023). Generation, accumulation, and distribution of Upper Paleozoic tight sandstone gas in the northeastern margin of the Ordos Basin. *Marine and Petroleum Geology* 156, 106463. doi:10.1016/j.marpetgeo.2023.106463

Wei, W., and Thomas, J. A. (2020). Elemental proxies for paleosalinity analysis of ancient shales and mudrocks. *Geochimica et Cosmochimica Acta* 287, 341–366. doi:10.1016/j.gca.2019.06.034

Worden, R. H., Griffiths, J., Wooldridge, L. J., Utley, J., Lawan, A., Muhammed, D., et al. (2020). Chlorite in sandstones. *Earth-Science Reviews* 204, 103105. doi:10.1016/j.earscirev.2020.103105

Wu, D., Liu, S. B., Chen, H. D., Lin, L., Yu, Y., Xu, C., et al. (2020). Investigation and prediction of diagenetic facies using well logs in tight gas reservoirs: evidences from the Xu-2 member in the Xinchang structural belt of the western Sichuan Basin, western China. *Journal of Petroleum Science and Engineering* 192, 107326. doi:10.1016/j.petrol.2020.107326

Xu, Z. Q., Yang, J. S., Li, H. Q., Wang, R. R., Cai, Z. H., et al. (2012). Indosinian collision-orogenic system of Chinese continent and its orogenic mechanism. *Acta Petrologica Sinica (in Chinese with English abstract)* 28 (6), 1697–1709.

Yang, L., Fan, A. P., Yang, R. C., Sun, Y. P., and Lenhardt, N. (2021). Sedimentary facies control on sandstone reservoir properties: A case study from the permian Shanxi Formation in the southern Ordos basin, central China. *Mar. Pet. Geol.* 129, 105083. doi:10.1016/J.MARPETGEO.2021.105083

Yang, N., Wang, G. W., Li, C. L., et al. (2014). Reservoir diagenetic facies of Bashijiqike Formation in Dabei gas field compartmentalization and quantitative evaluation. *Journal of China University of Petroleum* 38 (5), 18–24. (in Chinese with English abstract).

Yang, Z., Zou, C. N., Chen, J. J., Wu, S. T., Pan, S. Y., Ma, F., et al. (2021). Exploring petroleum inside or near the source kitchen": innovations in petroleum geology theory and reflections on hydrocarbon exploration in key fields. *Acta Petrolei Sinica (in Chinese with English abstract)* 42 (10), 1310–1324.

Yi, J. Z., Zhang, S. M., Cai, L. X., Chen, S. C., Luo, X., Yu, J. X., et al. (2022). Strata and sedimentary filling characteristics of the lower jurassic Lianggaoshan Formation and its hydrocarbon exploration in eastern Sichuan Basin. *Journal of Jilin University (Earth Science Edition)* 52 (3), 795–815. (in Chinese with English abstract). doi:10.13278/j.cnki.jjuese.20210429

Yokoyama, M., Liu, Y. Y., Halim, N., and Otofuji, Y. i. (2001). Paleomagnetic study of upper jurassic rocks from the Sichuan Basin: tectonic aspects for the collision between the Yangtze block and the north China block. *Earth and Planetary Science Letters* 193, 273–285. doi:10.1016/s0012-821x(01)00498-8

Yu, X., Yang, Y. X., Zhou, H. H., Luo, B., Luo, L., Luo, X., et al. (2023). Genetic mechanism of tight sandstone reservoir of lacustrine - delta sand-mud interlayer in Lianggaoshan Formation of Jurassic, eastern Sichuan Basin. *Natural Gas Geoscience (in Chinese with English abstract)* 34 (9), 1595–1611.

Zhang, C., Sun, W., Gao, H., Xi, T. D., and He, Q. (2014). Reservoir diagenetic facies and porosity evolution pathways of chang 8 formation in huachi, Ordos basin. *Earth Science (in Chinese with English abstract)* 39 (4), 411–420.

Zhang, D. W. (2021). Development prospect of natural gas industry in the Sichuan Basin in the next decade. *Natural Gas Industry (in Chinese with English abstract)* 41 (8), 34–45.

Zhang, D. W., and Yang, Y. (2022). Exploration potential and development direction of continental tight sandstone gas in the Sichuan Basin. *Natural Gas Industry (in Chinese with English abstract)* 42 (1), 1–11.

Zhang, F., Jiang, Z. X., Sun, W., Li, Y., Zhang, X., Zhu, L., et al. (2019). A multiscale comprehensive study on pore structure of tight sandstone reservoir realized by nuclear magnetic resonance, high pressure mercury injection and constant-rate mercury injection penetration test. *Marine and Petroleum Geology* 109, 208–222. doi:10.1016/j.marpetgeo.2019.06.019

Zhang, L. Q., Li, J. J., Wang, W., Li, C. Y., Zhang, Y. J., Jiang, S., et al. (2022). Diagenetic facies characteristics and quantitative prediction via wireline logs based on machine learning: a case of Lianggaoshan tight sandstone, fuling area, Southeastern Sichuan Basin, Southwest China. *Frontiers in Earth Science* 10, 1018442. doi:10.3389/feart.2022.1018442

Zhao, C. J., Jiang, Y. L., and Wang, L. J. (2022). Data-driven diagenetic facies classification and well-logging identification based on machine learning methods: a case study on Xujiahe tight sandstone in Sichuan Basin. *Journal of Petroleum Science and Engineering* 217, 110798. doi:10.1016/j.petrol.2022.110798

Zhao, Z. J., Zhou, H., Chen, X., Liu, Y. H., Zhang, Y. B., Liu, Y. E., et al. (2012). Sequence lithofacies paleogeography and favorable exploration zones of the Permian in Sichuan Basin and adjacent areas, China. *Acta Petrolei Sinica (in Chinese with English abstract)* 33 (S2), 35–51.

Zheng, C., Xu, C. H., Brix, M. R., and Zhou, Z. (2019). Evolution and provenance of the Xuefeng intracontinental tectonic system in South China: constraints from detrital zircon fission track thermochronology. *Journal of Asian Earth Sciences* 176, 264–273. doi:10.1016/j.jseaes.2019.02.012

Zheng, D. Y., Hou, M. C., Chen, A. Q., Zhong, H., Qi, Z., Ren, Q., et al. (2022). Application of machine learning in the identification of fluvial-lacustrine lithofacies from well logs: a case study from Sichuan Basin, China. *Journal of Petroleum Science and Engineering* 215, 110610. doi:10.1016/j.petrol.2022.110610

Zheng, D. Y., Wu, S. X., and Hou, M. C. (2021). Fully connected deep network: an improved method to predict TOC of shale reservoirs from well logs. *Marine and Petroleum Geology* 132, 105205. doi:10.1016/j.marpetgeo.2021.105205

Zheng, R. C., Geng, W., Zhou, G., Han, Y. L., Wang, H. H., and Wen, H. G. (2007). Diagenesis and diagenetic facies of chang 6 sandstone of yanchang formation in baibao area, Ordos basin. *Lithologic Reservoirs (in Chinese with English abstract)* 19 (2), 1–8.

Zhu, H., Yang, G., Yuan, B. G., Ying, D. L., Dai, X., Zhou, H. F., et al. (2018). Geological conditions, resource potential and exploration direction of conventional gas in Sichuan Basin. *Natural Gas Geoscience (in Chinese with English abstract)* 29 (10), 1475–1485.

Zhu, R. K., Zou, C. N., Mao, Z. G., Yang, H., Hui, X., Wu, S., et al. (2019). Characteristics and distribution of continental tight oil in China. *Journal of Asian Earth Sciences* 178, 37–51. doi:10.1016/j.jseaes.2018.07.020

Zou, C. N., Tao, S. Z., Zhou, H., Zhang, X. x., He, D. b., Zhou, C. m., et al. (2008). Genesis, classification, and evaluation method of diagenetic facies. *Petroleum Exploration and Development* 35 (5), 526–540. doi:10.1016/s1876-3804(09)60086-0

Zou, C. N., Yang, Z., Dong, D. Z., Zhao, Q., Chen, Z. H., Feng, Y. L., et al. (2022). Formation, distribution and prospect of unconventional hydrocarbons in source rock strata in China. *Earth Science (in Chinese with English abstract)* 47 (5), 1517–1533.

Zou, C. N., Zhang, G. S., Yang, Z., Tao, S., Hou, L., Zhu, R., et al. (2013). Concepts, characteristics, potential and technology of unconventional hydrocarbons: on unconventional petroleum geology. *Petroleum Exploration and Development* 40 (4), 413–428. doi:10.1016/s1876-3804(13)60053-1

Zou, J., Le, Y., Jin, T., Li, X. Q., Li, X. S., and Wei, T. Q. (2018). Genesis and sweet spot prediction of Jurassic tight sandstone reservoir in central Sichuan Basin. *Xinjiang Petroleum Geology (in Chinese with English abstract)* 39 (5), 555–560.